A CASE STUDY ON SUPPORT VECTOR MACHINES VERSUS ARTIFICIAL NEURAL NETWORKS

by

Wen-Chyi Lin

BS, Chung-Cheng Institute of Technology, 1998

Submitted to the Graduate Faculty of

School of Engineering in partial fulfillment

of the requirements for the degree of

Master of Science

University of Pittsburgh

2004

UNIVERSITY OF PITTSBURGH

SCHOOL OF ENGINEERING

This thesis was presented

by

Wen-Chyi Lin

It was defended on

July 21, 2004

and approved by

J. Robert Boston, Professor, Department of Electrical Engineering

Luis F. Chaparro, Associate Professor, Department of Electrical Engineering

Thesis Advisor: Ching-Chung Li, Professor, Department of Electrical Engineering

ABSTRACT

A CASE STUDY ON SUPPORT VECTOR MACHINES VERSUS ARTIFICIAL NEURAL NETWORKS

Wen-Chyi Lin, MS

University of Pittsburgh, 2004

The capability of artificial neural networks for pattern recognition of real world problems is well known. In recent years, the support vector machine has been advocated for its structure risk minimization leading to tolerance margins of decision boundaries. Structures and performances of these pattern classifiers depend on the feature dimension and training data size. The objective of this research is to compare these pattern recognition systems based on a case study. The particular case considered is on classification of hypertensive and normotensive right ventricle (RV) shapes obtained from Magnetic Resonance Image (MRI) sequences. In this case, the feature dimension is reasonable, but the available training data set is small, however, the decision surface is highly nonlinear.

For diagnosis of congenital heart defects, especially those associated with pressure and volume overload problems, a reliable pattern classifier for determining right ventricle function is needed. RV's global and regional surface to volume ratios are assessed from an individual's MRI heart images. These are used as features for pattern classifiers. We considered first two linear classification methods: the Fisher linear discriminant and the linear classifier trained by the Ho-Kayshap algorithm. When the data are not linearly separable, artificial neural networks with back-propagation training and radial basis function networks were then considered, providing

nonlinear decision surfaces. Thirdly, a support vector machine was trained which gives tolerance margins on both sides of the decision surface. We have found in this case study that the back-propagation training of an artificial neural network depends heavily on the selection of initial weights, even though randomized. The support vector machine where radial basis function kernels are used is easily trained and provides decision tolerance margins, in spite of only small margins.

TABLE OF CONTENTS

LIST OF TABLES

LIST OF FIGURES

ACKNOWLEDGMENTS

I would like to thank my advisor, Professor C. C. Li for his guidance and encouragement during this thesis. Also I would like to thank Professor J. R. Boston and Professor L. F. Chaparro, my committee members, for their helpful reviews and comments, Dr. M. Kaygusuz (Pediatric Cardiology, U. of Miami), Dr. R. Munoz and Dr. G. J. Boyle (Pediatric Cardiology, UPMC) for their suggestions and for providing their experimental data used in this thesis. Finally, let me give my gratitude to Ji-Ning Corporation, Taiwan, R.O.C for giving me a fellowship for my graduate study.

1.0 INTRODUCTION

1.1 BACKGROUND AND MOTIVATION

The capability of artificial neural networks for pattern recognition of real world problems is well known. With the increasing performance of modern computers and the urgent demand for classifiers accuracy, recently the support vector machine has been advocated for its structure risk minimization which gives tolerance margins of decision boundaries [1]. To compare these pattern recognition systems, a classification problem of hypertensive and normotensive right ventricle (RV) shapes obtained from Magnetic Resonance Image (MRI) sequences is considered [2].

Discovery and understanding of the structures in data is crucial in constructing classifiers. The separability of classes is a fundamental geometrical property and, therefore, attempting to derive linear discriminants is a useful first step in the exploration. We considered first two linear classification methods: the Fisher linear discriminant and the linear classifier trained by the Ho-Kayshap algorithm.

Consider a two-class (ω_1, ω_2) problem, if the data samples $\{\boldsymbol{x}\}$ are linearly separable, then there exists a weights vector $\mathbf{w}$ and a threshold b such that

$$y = \mathbf{w}^t x + b, \quad \begin{cases} \text{y} > 0, \text{ if } \boldsymbol{x} \in \omega_1 \\ \text{y} < 0, \text{ if } \boldsymbol{x} \in \omega_2 \end{cases} \qquad \text{(1-1).}$$

Fisher linear discriminant analysis [3] seeks directions of **w** that are most efficient for discrimination. By calculating within-class scatter matrix $\mathbf{S}_W$, between-class scatter matrix $\mathbf{S}_B$, and solving for a generalized eigenvalue problem, we will find the associated eigenvectors. Projecting the data $\boldsymbol{x}$ onto the principal eigenvector, we can immediately tell from the results whether the data are linearly separable or not. The Ho-Kashyap training algorithm [4] uses the gradient descent procedure trying to find a weight vector **w** and a threshold **b** by minimizing the criterion function

$$J(w,b) = \|\mathbf{Yw} - \mathbf{b}\|^2 \qquad (1\text{-}2),$$

where

$$\mathbf{Y} = \begin{bmatrix} 1_1 & \mathbf{X_1} \\ -1_2 & -\mathbf{X_2} \end{bmatrix} \qquad (1\text{-}3),$$

and $\mathbf{X_1}$ and $\mathbf{X_2}$ are the training sample subsets of class 1 and class 2, respectively. If the samples are linearly separable, there exists a **w** and a **b** > 0 such that

$$\mathbf{Yw} = \mathbf{b} > 0 \qquad (1\text{-}4).$$

A decision hyperplane is given by

$$\mathbf{w}^t\mathbf{x} + \mathbf{b} = 0 \qquad (1\text{-}5).$$

When the data is not linearly separable, artificial neural networks with hidden units may be trained. Learning the nonlinear decision surface is the key power provided by artificial neural networks. Feedforward multilayered artificial neural networks with sigmoidal nonlinearity in artificial neurons are the most commonly used networks along with the back-propagation training. Alternatively, radial basis functions are used in the hidden layer of the network.

To find an "optimal" decision surface which separates patterns of two classes, a support vector machine (SVM) provides us a powerful tool to achieve this task. Using the kernel mapping technique, a SVM can be trained to minimize the structural risk and to separate either linearly or nonlinearly separable data. It gives tolerance margins on both sides of the decision surface. The support vectors are those transformed training patterns that are closest to the separating surface (Figure 1-1).

These different types of pattern classifiers have their separating characteristics and different degrees of trainability depending on the nature of the problem, data dimensionality and the available training data. This project undertakes a case study on classification of these pattern classifiers.

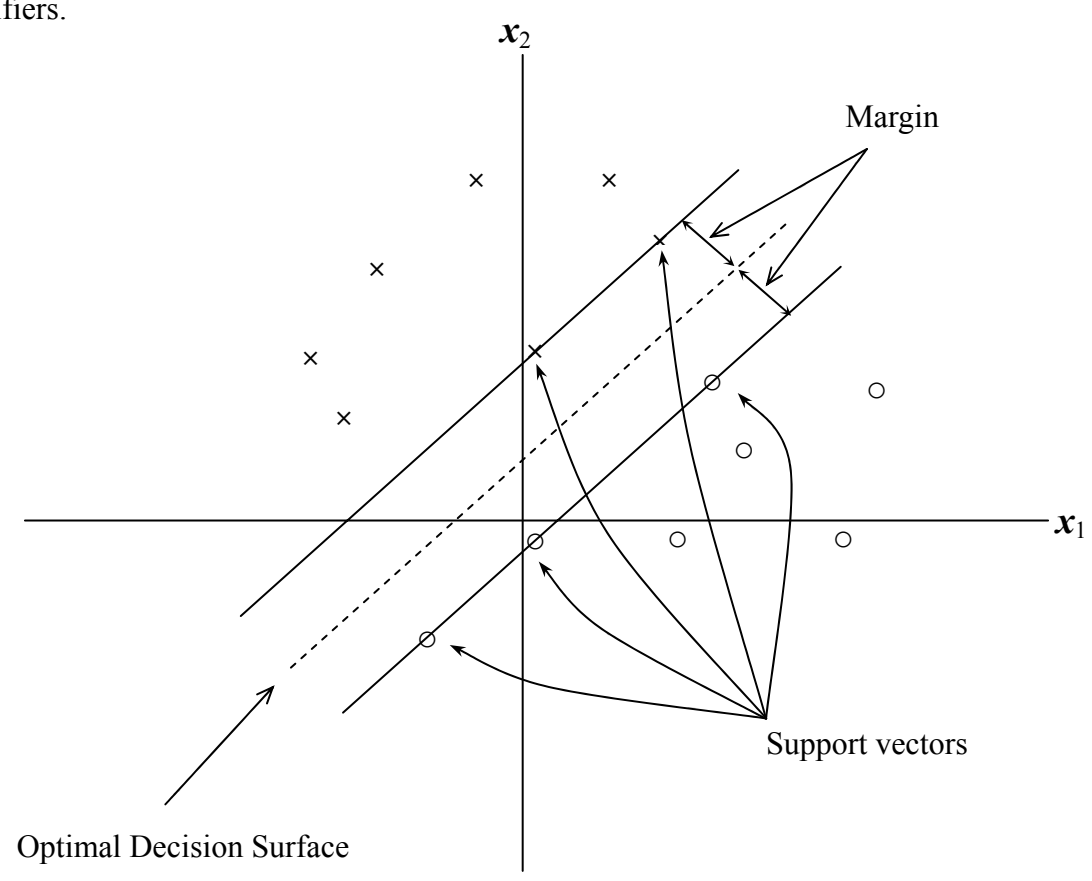

Figure 1-1 The Optimal Decision Surface that Separates Training Data of Two Classes with the Maximal Margin.

1.2 STATEMENT OF THE PROBLEM

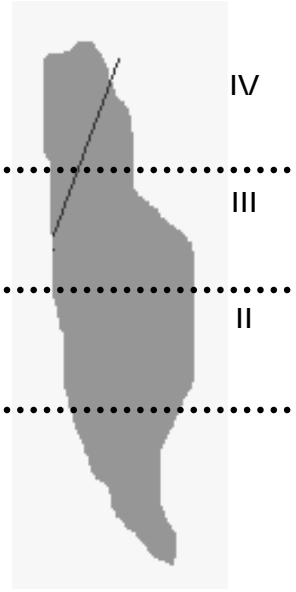

Figure 1-2 Division of RV into 4 Different Regions.

The specific pattern classifier under consideration is a biomedical pattern recognition problem. Consider that a 3 dimensional right ventricle is reconstructed from a cardiac MRI sequence. The shape of the right ventricle contains the information pertaining to the normality or the congenital heart defect. A quantitative classification of the RV shape has been suggested [2] that utilizes measurement on surface-to-volume ratio. A RV is divided into four regions and each is separated by 25% of the distance from the apex to the pulmonary valve as shown in Fig. 1-2. The volume and surface area of each region are calculated to provide four regional surface/volume (S/V) ratios, and the global surface/volume ratio of the whole RV is also computed. They together provide five features to be used in pattern classification to detect congenital heart defects, especially those associated with pressure and volume overload. Hence, the hypertensive case is to be differential from the normotensive case, base on these five features.

Training data are provided by Dr. Munoz and Dr. Kaygusuz, they were extracted from MRI sequences of RV plastic casts. Their previous studies have shown that S/V ratio decreases in general as RV becomes hypertensive. They trained an artificial neural network with two hidden layers each having four neurons. Their result indicates that one of these patterns was incorrectly classified. This is obviously a highly nonlinear separation problem.

In this thesis, we study the training of linear dicriminant functions, artificial neural networks and SVMs, using these data as a case study. We hope to understand the RV data structure, to reduce the number of the weights to be trained and to increase the classification accuracy, in particular, to compare the performance of the trained feedforward artificial neural network and that of the trained support vector machine.

1.3 OUTLINE

This thesis is composed of five chapters. The present chapter has introduced the background and research objective for the case study on support vector machines versus artificial neural networks. Chapter 2 deals with the problem of linear separability, both Fisher linear discriminants analysis and the Ho-Kashyap training procedure are reviewed and experimented. Chapter 3 discusses feedforward artificial neural networks as well as radial basis functions network where sigmoidal and Gaussian functions are used respectively as nonlinear functions in neural units. In each case, Jackknife training and error estimation are applied. Support vector machines are trained with both sigmoidal and Gaussian kernel functions as discussed in Chapter 4. Experiment results are presented in each Chapter. In chapter 5, discussions and conclusions are given, as well as the issues to be explored further.

2.0 LINEAR DISCRIMINANT FUNCTIONS

2.1 INTRODUCTION

The main goal of a classification problem is to find a classifier that can predict the label of new unseen data correctly. In practice, the problem often begins with a finite training set presumed to represent the expected input. Important information of the problem can be obtained by learning from the training data. Separability of data is a fundamental geometrical property; therefore, when we construct a classifier for linearly or nonlinearly separable data, it is useful to explore linear discriminant functions as the first step.

Dimensionality of the data is one of the recurring problems we face when applying statistical approaches to pattern recognition. Procedures that are analytically or computationally accessible in low-dimensional spaces may become totally impractical in high-dimensions spaces. The classical Fisher's discriminant analysis is to examine separation of data in a high dimensional space by projecting them into an appropriate line, the principal axis of the data.

In the next section, Fisher's method is briefly reviewed. In Section 2.3, the Ho-Kashyap training procedure is reviewed for the 2-class problem. If the sample patterns are linearly separable, then any of the two methods will produce a linear classifier. However, if the sample data are not linearly separable, then it indicates the nature of the possible non-linear separation of the data. Section 2.4 gives a summary of the experimental results of these two methods when applied to the RV shape data.

2.2 FISHER LINEAR DISCRIMINANTS

Fisher's linear discriminant analysis clusters patterns of the same class and separates patterns of different classe by maximizing the ratio of between-class variance to within-class variance. Patterns are projected from the *d*-dimensional feature space (where ***d*** is the number of features used) to a line. By turning the line around, one would find a directed line on which the projected samples are well separated or not.

Let us consider a 2-class problem that there is a set of $\boldsymbol{N}$ d-dimensional samples $\boldsymbol{x}_1, \ldots, \boldsymbol{x}_N$, $\boldsymbol{N}_i$ of which are in the subset $\boldsymbol{X}_i$ labeled by ω_i ($\boldsymbol{i}$ = 1,2), and $\boldsymbol{N}_1 + \boldsymbol{N}_2 = \boldsymbol{N}$. With a d-dimensional weight vector $\boldsymbol{w}$, we calculate the scalar

$$\boldsymbol{y} = \boldsymbol{w}^T\boldsymbol{x} \qquad (2\text{-}1),$$

and hence obtain a corresponding set of $\boldsymbol{N}$ 1-dimensional samples $\boldsymbol{y}_1; \ldots; \boldsymbol{y}_N$ which are divided into the subsets Ψ_1 and Ψ_2. Based on Eq. (2-1), the sample mean for the projected points is

$$\tilde{m}_i = \frac{1}{\mathrm{N}_i} \sum_{y_k \in \Psi i} y_k = w^T m_i \qquad (2\text{-}2),$$

where $m_i = \frac{1}{\mathrm{N}_i} \sum_{x_k \in X_i} x_k$. The scatter for the projected samples labeled ω_i is given by

$$\tilde{s}_i^2 = \sum_{y \in \Psi i} (y - \tilde{m}_i)^2 \qquad (2\text{-}3).$$

The Fisher's linear discriminant function is defined as the linear function $\boldsymbol{w}^{\mathrm{T}}\boldsymbol{x}$ for which the criterion function

$$J(\mathrm{w}) = \frac{\left|\tilde{m}_1 - \tilde{m}_2\right|^2}{\tilde{s}_1^2 + \tilde{s}_2^2} \qquad (2\text{-}4),$$

is maximum, where $\left|\tilde{m}_1 - \tilde{m}_2\right| = \left|\mathbf{w}^{\mathrm{T}}(\mathbf{m_1} - \mathbf{m_2})\right|$ according to Eq.(2-2). To derive J as an explicit

function of **w**, we define the scatter matrices $\boldsymbol{S}_i$, the within-class scatter matrix $\boldsymbol{S}_W$ and the between-class scatter matrix $\boldsymbol{S}_B$ as follows

$$S_i = \sum_{x_k \in X_i} (\mathrm{x_k} - \mathrm{m_i})(\mathrm{x_k} - \mathrm{m_i})^T \qquad (2\text{-}5),$$

$$\boldsymbol{S}_W = \boldsymbol{S}_1 + \boldsymbol{S}_2, \qquad (2\text{-}6),$$

and $$\boldsymbol{S}_B = (\mathbf{m}_1 - \mathbf{m}_2)(\mathbf{m}_1 - \mathbf{m}_2)^{\mathrm{T}}. \qquad (2\text{-}7).$$

Using Eq.(2-2), Eq.(2-3) and the definitions given above, we can obtain

$$\tilde{s}_1^2 + \tilde{s}_2^2 = \mathbf{w}^{\mathbf{T}} \boldsymbol{S}_W \mathbf{w} \qquad (2\text{-}8),$$

and

$$\left|\tilde{m}_1 - \tilde{m}_2\right|^2 = \mathbf{w}^{\mathbf{T}} \boldsymbol{S}_B \mathbf{w} \qquad (2\text{-}9).$$

By substituting these expressions into Eq.(2-4), the criterion function J can be written as

$$\boldsymbol{J}(\mathbf{w}) = \frac{\mathbf{w}^{\mathbf{T}} S_{\mathbf{B}} \mathbf{w}}{\mathbf{w}^{\mathbf{T}} S_{\mathbf{w}} \mathbf{w}} \qquad (2\text{-}10),$$

Maximizing $\boldsymbol{J}$ by taking $\frac{\partial J}{\partial \mathrm{w}} = 0$ leads to

$$\boldsymbol{S}_{\mathbf{w}} \mathbf{w}(\mathbf{w}^{\mathbf{T}} \mathbf{S}_{\mathbf{B}} \mathbf{w}) = \boldsymbol{S}_{\mathbf{B}} \mathbf{w}(\mathbf{w}^{\mathbf{T}} \mathbf{S}_{\mathbf{w}} \mathbf{w}) \qquad (2\text{-}11).$$

Let $\lambda = (\mathbf{w}^{\mathbf{T}} \mathbf{S}_{\mathbf{B}} \mathbf{w})\,(\mathbf{w}^{\mathbf{T}} \mathbf{S}_{\mathbf{w}} \mathbf{w})^{-1}$ which is a scalar, then

$$\lambda\, \mathbf{w} = (\mathbf{S}_{\mathbf{w}}^{-1} \mathbf{S}_{\mathbf{B}}) \mathbf{w} \qquad (2\text{-}12),$$

becomes an eigenvector problem. From Eq. (2-7), since

$$\mathbf{S}_{\mathbf{B}} \mathbf{w} = (\mathbf{m}_1 - \mathbf{m}_2)(\mathbf{m}_1 - \mathbf{m}_2)^{\mathrm{T}} \mathbf{w} = (\mathbf{m}_1 - \mathbf{m}_2)\, k \qquad (2\text{-}13),$$

where $k = (\mathbf{m}_1 - \mathbf{m}_2)^{\mathrm{T}} \mathbf{w}$ **is a scalar,** $\mathbf{S}_{\mathbf{B}} \mathbf{w}$ has the direction of $(\mathbf{m}_1 - \mathbf{m}_2)$,

$$\lambda \mathbf{w} = k \mathbf{S}_{\mathbf{w}}^{-1}(\mathbf{m}_1 - \mathbf{m}_2) \qquad (2\text{-}14).$$

The nonsingular $\boldsymbol{S_W}$ gives the normalized solution of the weight vector **w** [7]

$$\mathbf{w} = S_{\mathbf{w}}^{-1}(\mathbf{m}_1 - \mathbf{m}_2). \qquad (2\text{-}15).$$

Using the weight vector, all the sample patterns X's are mapped onto a line y, forming two subsets φ_1 and φ_2 with maximum interest distance and minimum intraset distance. To identify a test pattern, compare the distance from the projected test pattern to each subsets φ_i, and the test pattern is identified with the closest training subsets φ_i.

For the sample data set of right ventricle shapes given in Appendix A, which consist of 11 normal and 12 abnormal (hypertensive, HTN) patterns, five Surface/Volume features (global S/V, 0-25%S/V, 25-50%S/V, 50%-75%S/V, and 75-100%S/V) form a 5-dimensional space. Figure 2-1 and Table 2-1 show the Fisher linear discriminant analysis result where projection y values are given. The computed weight vector, eigenvector, **w** is [0.1342 -0.0241 0.1931 0.9714 0.0230]^T. Note that the two subsets are not completely separated, and pattern 1 (Normal-2) and 14 (HTN-12) cannot be correctly placed. In the next section, we will try to apply the Ho-Kashyap algorithm to explore whether these two pattern classes can be linearly separated.

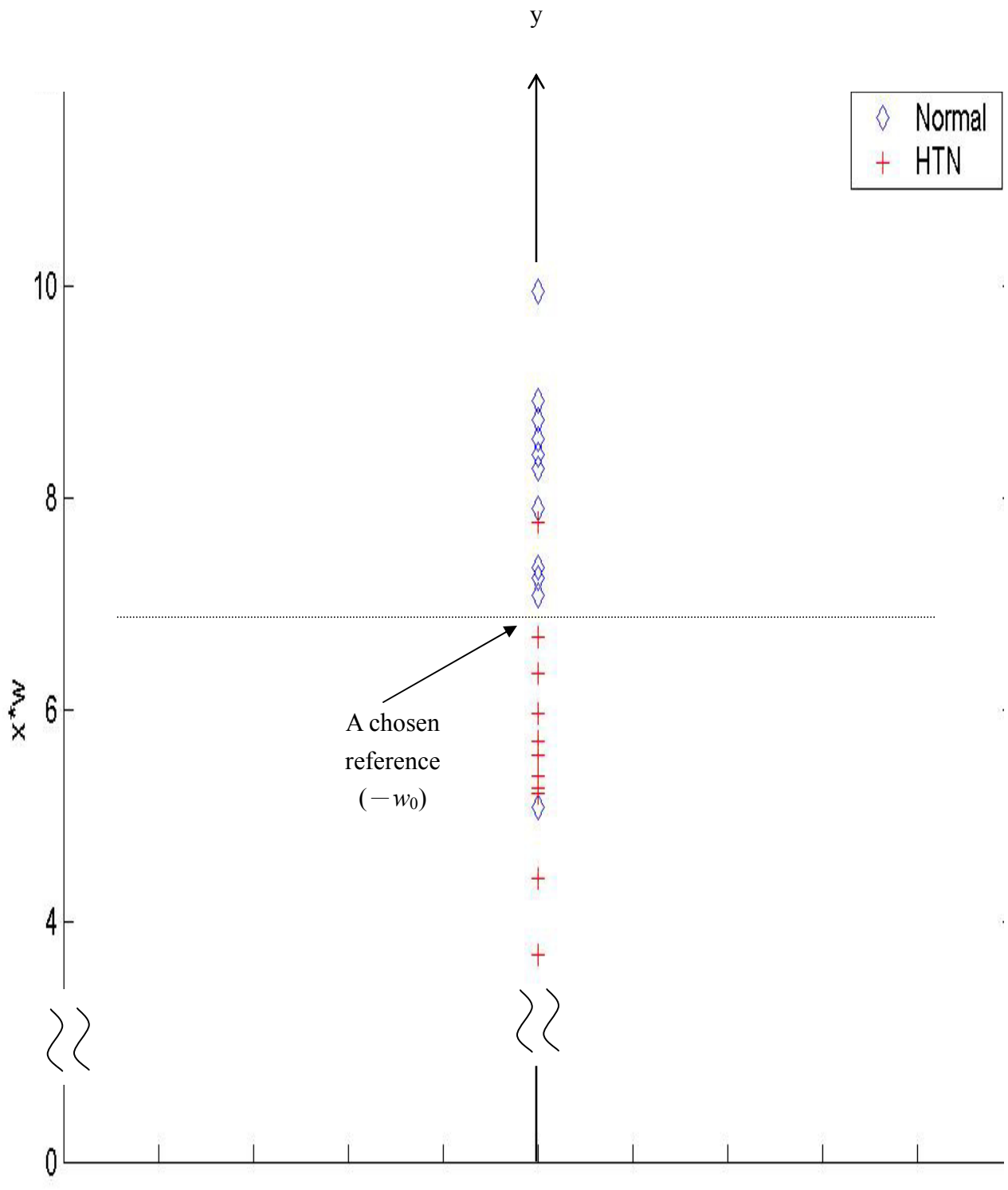

Figure 2-1 Fisher Linear Discriminant Analysis Result of 5-Feature of RV Shape Data.

Table 2-1 Fisher's Linear Discriminant Analysis Result of 5-Feature RV Shape Data.

Normal		HTN (abnormal)	
No.	Projection y	No.	Projection y
1	***5.0889***	12	6.6827
2	7.3383	13	5.2614
3	9.9437	14	***7.7649***
4	8.2679	15	5.3735
5	8.4051	16	5.2193
6	7.0860	17	5.5820
7	8.5550	18	5.2666
8	8.7387	19	5.7094
9	7.9029	20	6.3509
10	8.9088	21	4.4162
11	7.2511	22	3.6836
		23	5.9747

2.3 THE HO-KASHYAP TRAINING ALGORITHM

The Ho-Kashyap algorithm [4] combines the least mean squares errors and the gradient descent procedures to train a weight vector **w** by minimizing the criterion function

$$J(\mathbf{w},\mathbf{b}) = \|\mathbf{Y}\mathbf{w} - \mathbf{b}\|^2 \qquad (2\text{-}16),$$

where

$$\mathbf{Y} = \begin{bmatrix} 1_1 & \mathbf{X_1} \\ -1_2 & -\mathbf{X_2} \end{bmatrix} \qquad (2\text{-}17),$$

is the augmented pattern matrix, **w** is the augment weight vector with the threshold weight or

bias w_0 as its first component, and $\mathbf{b} > \mathbf{0}$. Let $\mathbf{Y}^+$ be the pseudo inverse of $\mathbf{Y}$. The training algorithm is stated as follows:

$$\mathbf{w}(1) = \mathbf{Y}^+\mathbf{b}(1), \quad \mathbf{b}(1) > \mathbf{0} \text{ but otherwise arbitrary}$$

$$\mathbf{e}(k) = \mathbf{Y}\mathbf{w}(k) - \mathbf{b}(k)$$

$$\mathbf{b}(k+1) = \mathbf{b}(k) + \eta(\mathbf{e}(k) + |\mathbf{e}(k)|), \quad 0 < \eta < 1$$

$$\mathbf{w}(k+1) = \mathbf{w}(k) + \eta\mathbf{Y}^+(\mathbf{e}(k) + |\mathbf{e}(k)|)$$

This algorithm yields a solution vector $\mathbf{w}^*$ for $\mathbf{Y}\mathbf{w}^* > 0$ in finite number of steps, if the training samples are linearly separable. If the training samples are not linearly separable, a non-positive $\mathbf{e}(k)$ will occur in finite number if steps (components of $\mathbf{e}(k)$ are all non-positive with at least one component to be negative); that indicates the nonlinear separability.

For the sample data set of right ventricle shapes given in Appendix A, and with $\eta = 0.1$ and $\mathbf{b}(1)$ given in Table 2-3, the algorithm terminates at iteration step 42 with an augmented weight vector $\mathbf{w}$ = [0.1077 0.2980 0.2183 0.1615 0.1731 0.1800], and indicates that the sample data are not linearly separable. Pattern No. 9 (Normal-13) and 22 (HTN-21) are incorrectly placed as shown in Table 2-2.

Table 2-2 Result of the Ho-Kashyap Training Procedure.

Training Result by Applying the Ho-Kashyap procedure (Iterations:42)	
Correct	1, 2, 3, 4, 5, 6, 7, 8, 10, 11, 12, 13, 14, 15, 16, 17, 18, 19, 20, 21, 23
Incorrect	9, 22

Table 2-3 Weights, Bias and Errors of the Ho-Kayshap Training Procedure.

Initial w	Final w	No	Initial b	Final b	Error e (1.0e-005 *)
0.5000	0.1077	1.	0.0158	5.6740	0.0000
0.5000	0.2980	2.	0.0164	7.6291	0.0000
0.5000	0.2183	3.	0.1901	12.4615	0.0000
0.5000	0.1615	4.	0.5869	9.9911	0.0000
0.5000	0.1731	5.	0.0576	9.0957	0.0000
0.5000	0.1800	6.	0.3676	9.3225	0.0000
Learning rate η		7.	0.6315	10.7204	0.0000
0.1		8.	0.7176	9.0691	0.0000
		9.	0.6927	10.6469	-0.3839
		10.	0.0841	12.2709	0.0000
		11.	0.4544	9.1324	0.0000
		12.	0.4418	7.5702	0.0000
		13.	0.3533	6.2437	0.0000
		14.	0.1536	8.8024	0.0000
		15.	0.6756	6.2492	0.0000
		16.	0.6992	6.8332	0.0000
		17.	0.7275	7.0763	0.0000
		18.	0.4784	6.5037	0.0000
		19.	0.5548	6.1664	0.0000
		20.	0.1210	7.1582	0.0000
		21.	0.4508	6.3121	0.0000
		22.	0.7159	3.6434	-0.6980
		23.	0.8928	6.6628	0.0000

2.4 SUMMARY

Both the Fisher's linear discriminant analysis and the Ho-Kashyap training algorithm indicate that the sample RV shape data are not linearly separable. Each experiment provides us with a weight vector resulting in 2 classification errors of the training. One normal pattern falls into the abnormal (HTN) region, and one HTN falls into the normal region. The condition of the application of the Ho-Kayshap procedure clearly indicates the nonlinear separability of the data which necessitates a nonlinear pattern classifier. We will study the use of artificial neural networks and support vector machines on classifying right ventricle shape data.

3.0 ARTIFICIAL NEURAL NETWORKS AND RADIAL BASIS FUNCTIONS

n artificial neural network (ANN) is an information processing system that employs certain characteristics of biological neural processors. It analyzes data by passing the data through a number of neural units which are interconnected and highly distributed. A neural network performs its processing by accepting inputs $\boldsymbol{x_i}$, which are then multiplied by a set of weights $\boldsymbol{w_i}$. A neuron transforms the sum of the weighted inputs nonlinearly into an output value, $\boldsymbol{y}$, by using a nonlinear activation function or transfer function, **T**, as shown in Figure 3-1, where T(s) is commonly represented by a sigmoidal function. A bias, w_0, is added to the neuron, it is then regarded as a weight, with a constant input of 1.

3.1 ARTIFICIAL NEURAL NETWORKS

We consider the feedforward multilayered perceptrons (MLPs), as shown in Figure 3-2, that have been widely used in many applications. Hornik et al [5] proved that a three-layered MLP with an unlimited number of neurons in the hidden layer can solve arbitrary nonlinear mapping problems. However, the problem of training an MLP is NP-complete. As a result, we often have a slow convergence problem when training an MLP. Moreover, the number of hidden layers, neurons in a hidden layer, and connectivity between layers must be specified before learning can begin.

Some statistical techniques have been recently borrowed for model selection [6] [7], but most of them involve time-consuming procedures for practical use. Therefore, the network architecture must be determined by trial and error. Practical methods for dynamic neural network architecture generation have been sought [8] [9] to conquer the difficulty in determining the architecture prior to training, However, these models do not specify in what sequence a hidden neuron should be added to give the maximum effect in improving the training process since they still suffer from serious interference during the training phase. Therefore, determination of a neural network architecture and fast convergence in training still remain to be important research topics in the neural network area.

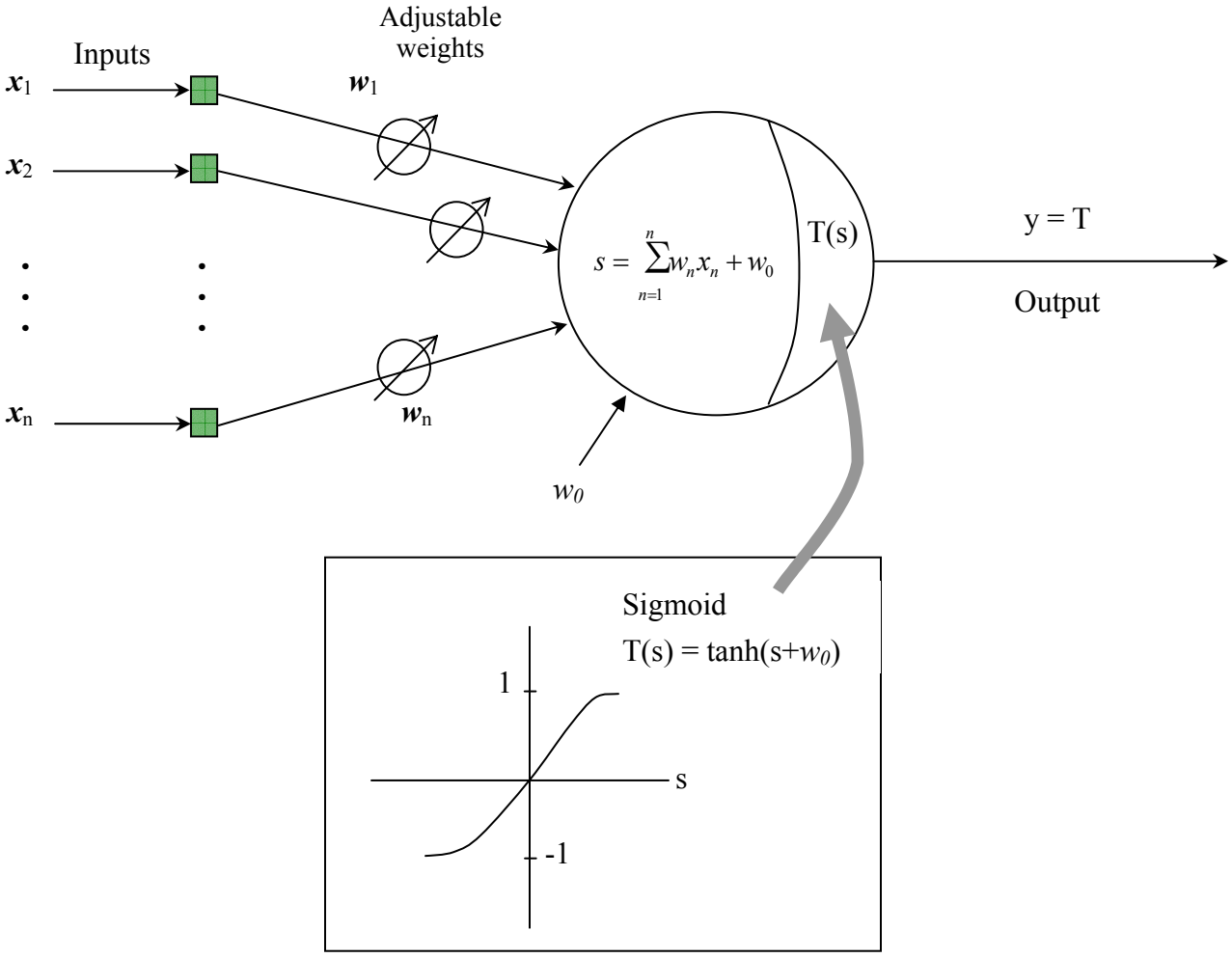

Figure 3-1 Block Diagram of an Artificial Neuron.

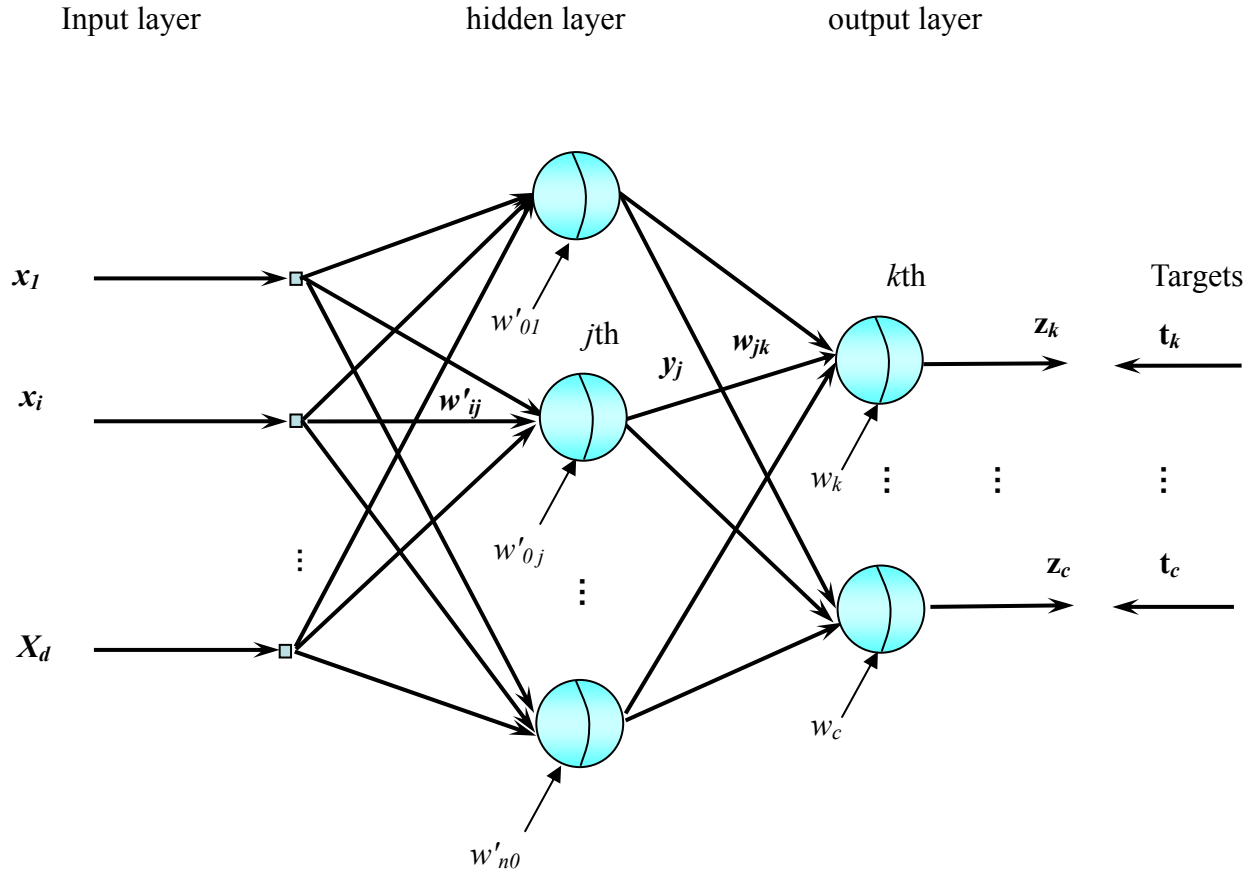

Figure 3-2 A Feedforward multilayed Artificial Neural Network.

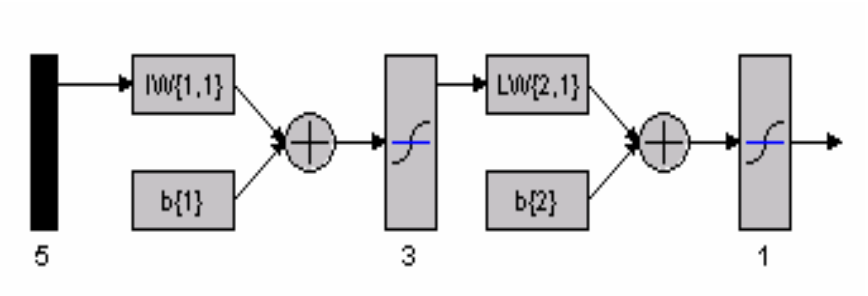

Figure 3-3 An Abbreviated Sketch of the (5-3-1) ANN Indicating 5 Inputs, 3 Hidden Units and 1 Output Neuron.

For classifying right ventricle shape data, Kaygusuz et al [2] trained a (5-4-4-2) artificial neural network with two hidden layers, each has four neurons, and two neurons in the output layer. For the 5-dimension features, there were [5 x 4 + 4] + [4 x 4 + 4] + [4 x 2 + 2] = 54 weight parameters to be trained, using 23 training patterns. There are too many weights in this model and it is hard to evaluate its performance. We consider only a single hidden layer with three hidden neurons and one output neuron in the output layer which suffices to implement the 2-class (normal class and hypertensive (HTN) class) problem under consideration. Figure 3-3 shows an abbreviated sketch of the (5-3-1) ANN indicating 5 inputs, 3 hidden units and 1 output neuron. This represents a significant reduction in the number of parameters to be trained ([5 x 3 +3] + [3 x 1 + 1] = 22).

As shown in Figure 3-1 an input vector is presented to the input layer. In hidden layers (only one is shown), each neuron computes the weighted sum of its inputs to form a net activation signal we denoted as *net*. That is, the net activation is the inner product of the inputs with the weights at the hidden unit. For simplicity, we augment both its input vector and weight vector by appending another input of $x_0 = 1$ and a bias, w_0, respectively, so we write for the *j*th neuron

$$net_j = \sum_{i=1}^{d} x_i w_{ij} + w_{j0} = \sum_{i=0}^{d} x_i w_{ij} \equiv \mathrm{w}_\mathrm{j}^\mathrm{T}\mathrm{x} \qquad (3\text{-}1),$$

where w_{ij} denotes the connection weight from the *i*th unit in the previous layer to the *j*th unit in the current layer. The output of this *j*th neuron is a nonlinear function (e.g., sigmoidal function) of its activation signal net_j, that is,

$$y_j = f(net_j) = f(\sum w_j^T x) \qquad (3\text{-}2).$$

We assume that the same nonlinearity is used in all hidden neurons. Each output neuron similarly computes its net activation signal based on the hidden neurons outputs in the hidden layer and gives its output

$$z_k = f(net_k) = f(\sum w_j^T x) \qquad (3\text{-}3),$$

This output nonlinearity may be a sign function or may even be a linear function. When there are *c* output neurons, we can think of the network as computing c discriminant functions $z_k = g_k(\mathbf{x})$, (k = 1, 2, …, c) that can classify an input to one of c classes according to which discriminant function is the largest. For our 2-class right ventricle shape problem, it is simpler to use a single output neuron and label a pattern by the sign of the output *z*.

3.1.1 Back-Propagation Training

Connection weights $\{\boldsymbol{w}_{ij}\}$ in multiple layers of the feedforward network are to be trained through the use of Q sample patterns of known classes. The back-propagation learning method starts with sending a training pattern to the input layer, passing the signals through the network and determining the output at the output layer. These c outputs z_k are then compared to their respective target values t_k,. their difference is treated as an error $e_k = t_k - z_k$. A criterion function $E(w) = \frac{1}{2}\sum_{k=1}^{c} e_k^2 = \frac{1}{2}\|\mathbf{e}\|^2$, where $\mathbf{e} = [e_1, e_2, \ldots, e_c]^T$, (or $E(w) = \frac{1}{2}\sum_{q=1}^{Q}\|e^q\|^2$ for a batch of Q training samples in one epoch) is minimized with respect to various connection weigths, where **t** and **z** are the target and the actual output vectors and **e** = **t** – **z**,

$$E(w) \equiv \frac{1}{2}\|\mathrm{e}\|^2 = \frac{1}{2}\sum_{k=1}^{c}(t_k - z_k)^2 = \frac{1}{2}\|\mathrm{t}-\mathrm{z}\|^2 \qquad (3\text{-}4),$$

The back-propagation learning rule [10] is based on the gradient descent. The weight vector w in each layer is initialized with random values, and then they are iteratively updated in a direction that will reduce the error criterion *E*

$$\mathrm{w}(k+1) = \mathrm{w}(k) + \Delta\mathrm{w}(k) \qquad (3\text{-}5),$$

$$\Delta\mathrm{w} = -\eta\frac{\partial E}{\partial \mathrm{w}} \qquad (3\text{-}6),$$

or in component form

$$\Delta w_{pq} = -\eta\frac{\partial J}{\partial w_{pq}} \qquad (3\text{-}7),$$

where η is the learning rate ($0 < \eta < 1$). The iteration k denotes the particular *k*th sample pattern presentation (or the *k*th epoch pattern presentation in a batch mode).

Consider the weight vector in the *l*th layer, for the weight w_{ij}^{l}, connecting to its *j*th neuron from the *i*th neuron of the (*l*-1)th layer,

$$\frac{\partial E}{\partial w_{ij}^{l}} = \frac{\partial E}{\partial net_j}\frac{\partial net_j}{\partial w_{ij}} = \delta_j^{l} y_i^{l-1} \qquad (3\text{-}8),$$

where y_i^{l-1} denotes the output of the *i*th neuron in the (*l*-1) layer. For output neuron *j*

$$\delta_j^{q} = \frac{\partial E}{\partial net_j} = -(t_j - z_j) f'(net_j) \qquad (3\text{-}9).$$

and for hidden neuron *j* in layer *l*,

$$\delta_j^q = \frac{\partial E}{\partial net_j} = f'(net_j)\sum_k \delta_k^{l+1} w_{jk} \qquad (3\text{-}10).$$

3.1.2 ANN Trained for Right Ventricle Shape Data

For all 23 samples of right ventricle shape data, a simple 3-layer neural network with 3 hidden neurons and 1 output neuron was successfully trained. There are many variations to the basic back-propagation training algorithm provided by Matlab [11]. Here we use **Tansig** as transfer function and **MSE** as our performance function. Two learning functions are used when training the ANN, one is **Learngdm** (with momentum) and the other is **Learngd** (without momentum).

Learngdm, the gradient descent with momentum computes the weight change $\Delta \mathbf{w}_j^l$ (including Δw_0**)** for a given neuron, with learning rate η and momentum constant α, according to the algorithm:

$$\Delta \mathbf{w}_j^l(k) = -(1-\alpha)\eta \frac{\partial E}{\partial \mathbf{w}_j^l} + \alpha \Delta \mathbf{w}_j^l(k-1) \qquad (3\text{-}11),$$

Learngd, the gradient descent without momentum computes the weight Δw_j^l for a given neuron with learning rate η, but without the momentum term ($\alpha = 0$).

$$\Delta \mathbf{w}(m+1) = -\eta \frac{\partial E}{\partial \mathbf{w}_j^l}(m) \qquad (3\text{-}12).$$

The initial weights were chosen at random (as shown in Table 3-1), and the learning rate η was set at 0.01. The training without momentum took more than 1000 epochs to converge. The final

weight vectors and bias values are given in Table 3-2. Training with momentum (with $\alpha = 0.01$) was much faster, it took only 100 epochs (Initial weights are shown in Table 3-3). The learning curve is shown in Figure 3-4. The trained weight vectors and bias values are given in Table 3-4.

Table 3-1 Initial Weights of the ANN Trained without Momentum by 23 RV Shape Samples.

ANN Initial Weights without Momentum Initial learning rate η = 0.01
Iw{1,1}-Weight to layer 1 from input 1
[-0.077737 -0.050193 -0.13225 0.13963 -0.26674; 0.32237 0.10099 -0.1029 -0.2897 0.12837; -0.30984 -0.13526 -0.089258 -0.32776 -0.02444]
Iw{2,1}-Weight to output layer
[1.3717 -0.10802 -0.25842]
b{1}-Bias to layer 1
[6.0289; -2.0764; 4.7147]
b{2}-Bias to layer 2
[0]

Table 3-2 Final Weights of the ANN Trained without Momentum by 23 RV Shape Samples.

ANN Final Weights without Momentum Initial learning rate η = 0.01
Iw{1,1}-Weight to layer 1 from input 1
[0.85477 0.43875 -0.18022 0.83995 0.14437; -0.16995 1.8856 -0.22309 0.6157 -1.2552; -2.7223 -0.57671 1.0751 -0.084569 0.35655]
Iw{2,1}-Weight to output layer
[5.0162 -9.8906 -12.925]
b{1}-Bias to layer 1
[-4.9191; -1.1093; 14.9876]
b{2}-Bias to layer 2
[5.0975]

Figure 3-4 Learning Curve (with momentum) of ANN Trained by 23 Samples.

Table 3-3 Initial Weights of the ANN Trained with Momentum by 23 RV Shape Samples.

ANN Initial Weights with Momentum Initial learning rate η = 0.01, α = 0.01
Iw{1,1}-Weight to layer 1 from input 1
[0.40002 -0.0049052 -0.016354 -0.076307 0.2381; -0.20434 0.11711 -0.1547 0.13623 0.115; 0.096493 0.093209 0.12271 0.40942 -0.18571]
Iw{2,1}-Weight to output layer
[-0.21634 0.99912 0.95653]
b{1}-Bias to layer 1
[-5.8869; -0.30297; -1.6229]
b{2}-Bias to layer 2
[0]

Table 3-4 Final Weights of the ANN Trained with Momentum by 23 RV Shape Samples.

ANN Final Weights with Momentum Initial learning rate η = 0.01, α = 0.01
Iw{1,1}-Weight to layer 1 from input 1
[0.43221 -2.9578 9.1507 0.70229 -2.6536; -0.52917 0.36766 0.29635 0.40206 1.1181; 0.25125 1.2348 0.52256 0.111 0.45395]
Iw{2,1}-Weight to output layer
[11.1691 12.949 -5.3405]
b{1}-Bias to layer 1
[3.5168; -12.5569; 4.815]
b{2}-Bias to layer 2
[-5.5975]

3.1.3 Jackknife Training and Error Estimation

Table 3-5 shows a subset of training data which we found can be used to successfully train an ANN that correctly classifies the rest of the RV patterns. This was found by trial and error using different combinations of subsets of RV patterns to train an ANN until no error was found in the testing phase. Pattern Normal_2 and pattern HTN_15 were included because they were misclassified by Fisher's linear discriminant. Now they are correctly classified. This gives a different satisfactory classifier. To gain a clear idea of the classification error rate, Jackknife Error Estimation was analyzed.

Table 3-5: 14 Training Subsets (Normal: 7 HTN: 7) and Trained Results at 30 Epochs.

No	Pattern#	Output	Ideal Output
1	Normal_2	1	1
2	Normal_3	1	1
3	Normal_4	1	1
5	Normal_6	1	1
6	Normal_7	1	1
7	Normal_8	1	1
11	Normal_24	1	1
1	HTN_9	***-1***	***-1***
3	HTN_12	***-1***	***-1***
5	HTN_15	***-1***	***-1***
7	HTN_17	***-1***	***-1***
8	HTN_18	***-1***	***-1***
9	HTN_19	***-1***	***-1***
10	HTN_20	***-1***	***-1***

The whole set of twenty three samples are divided into ten groups. Each time, one of the groups is put aside while the other nine are used to train an ANN, then we test the ANN using the untrained one. **Learngdm**, gradient descent with momentum, training program was used in adaptive learning ten times, and the trained classifiers were tested to give the results in Table 3-6. The False Positives and False Negatives are given in Table 3-7, their averages are summarized below:

$$\text{False Positive:} \quad \frac{1}{10} \times \frac{6}{11} = \frac{6}{110} = 0.0545$$

$$\text{False Negative:} \quad \frac{1}{10} \times \frac{5}{12} = \frac{5}{120} = 0.0417$$

Table 3-6 Jackknife Training and Error Estimates (with Momentum).

Jackknife Training and Error Estimates (with Momentum) Parts: 10 Hidden Neurons: 3 Output: 1 Features: 5										
No	Training data number			Testing data set			Training		Test Results *Normal:1 HTN:-1*	
	Normal	HTN	Total	Normal	HTN	Total	Wrong	Epochs	Correct	Wrong
1	10	11	21	#2	#9	2		21	0	N#2 H#9
2	10	11	21	#3	#11	2		36	2	0
3	10	11	21	#4	#12	2	N#2	523	1	N#4
4	10	11	21	#5	#14	2		126	2	0
5	10	11	21	#6	#15	2		45	2	0
6	10	11	21	#7	#16	2		64	1	N#7
7	10	11	21	#8	#17	2		142	2	0
8	10	10	20	#10	#18#19	3		465	2	H#18
9	10	10	20	#13	#20#21	3	N#2 H#12 H#18	278	2	H#20
10	9	11	20	#23#24	#22	3		37	2	N#24

Table 3-7 False Positive and Negative Rates of Jackknife Training and Error Estimates of the ANN classification of RV Shape Data (using Learngdm in training).

Times	N: normal H: HTN	Test Result		Error Rate	Times	N: normal H: HTN	Test Result		Error Rate	Times	N: normal H: HTN	Test Result		Error Rate
1	True	N	H		**2**	True	N	H		**3**	True	N	H	
	N(11)	**10**	**1**	**1/11**		N(11)	**11**	**0**	**0**		N(11)	**9**	**2**	**2/11**
	H(12)	**1**	**11**	**1/12**		H(12)	**0**	**12**	**0**		H(12)	**0**	**12**	**0**
4	True	N	H		**5**	True	N	H		**6**	True	N	H	
	N(11)	**11**	**0**	**0**		N(11)	**11**	**0**	**0**		N(11)	**10**	**1**	**1/11**
	H(12)	**0**	**12**	**0**		H(12)	**0**	**12**	**0**		H(12)	**0**	**12**	**0**
7	True	N	H		**8**	True	N	H		**9**	True	N	H	
	N(11)	**11**	**0**	**0**		N(11)	**11**	**0**	**0**		N(11)	**10**	**1**	**1/11**
	H(12)	**0**	**12**	**0**		H(12)	**1**	**11**	**1/12**		H(12)	**3**	**9**	**3/12**
10	True	N	H											
	N(11)	**11**	**0**	**1/11**										
	H(12)	**0**	**12**	**0**										

Next, we changed **learngdm** to **learngd** (the gradient descent without momentum) in training and then went through the Jackknife error estimation again. The results are given in Table 3-8 and Table 3-9. The average False Positive and average False Negative are

$$\text{False Positive:} \quad \frac{1}{10} \times \frac{5}{11} = \frac{5}{110} = 0.0454$$

$$\text{False Negative:} \quad \frac{1}{10} \times \frac{5}{12} = \frac{5}{120} = 0.0417$$

In this case, the False positive rate is slightly decreased; however, several patterns could not lead to successful training or be classified correctly in testing.

Table 3-10 shows a supposed "optimal" training data. Such "difficult" patterns were picked out in both cases, as marked by V in Table 3-10. These 11 samples were pooled together for another training. The training without momentum was successful but the speed of convergence was very slow. With the initial weights randomly chosen as given in Table 3-11, all RV patterns were correctly classified; the resulting weight vectors and bias values are given in Table 3-12. The training with momentum was faster, it took only 2840 epochs as shown in the learning curve in Figure 3-5, however, misclassified one pattern in testing. Figure 3-6 shows the training patterns in the x1-x2 (Global S/V vs. 0-25%S/V) plane. From the plot we can see that these patterns are located close to the border of the two classes and are expected to be difficult to train. We call this subset as "optimal" training subset. If we can successfully train an ANN with these samples, we expect the testing performance would show the least error rate. This subset lies inside the subset of 14 samples given in Table 3-5 but obtained other than trial-and-error.

Table 3-8 Jackknife Training and Error Estimates (without Momentum).

Jackknife Training and Error Estimates (without Momentum) Parts: 10 Hidden Neurons: 3 Output: 1 Features: 5										
No	Training data number			Testing data set			Training		Test Results *Normal:1 HTN:-1*	
	Normal	HTN	Total	Normal	HTN	Total	Wrong	Epochs	Correct	Wrong
1	10	11	21	#2	#9	2		50000	0	N#2 H#9
2	10	11	21	#3	#11	2		50000	1	N#3
3	10	11	21	#4	#12	2		50000	0	N#4 H#12
4	10	11	21	#5	#14	2		50000	2	0
5	10	11	21	#6	#15	2		50000	2	0
6	10	11	21	#7	#16	2		50000	1	N#7
7	10	11	21	#8	#17	2		50000	2	0
8	10	10	20	#10	#18 #19	3	H#12	50000	2	H#19
9	10	10	20	#13	#20 #21	3		50000	3	0
10	9	11	20	#23 #24	#22	3		50000	2	N#24 H#22

Table 3-9 False Positive and Negative Rates of Jackknife Training and Error Estimates of the ANN classification of RV Shape Data (using Learngd in training).

Times	N: normal H: HTN	Test Result		Error Rate	Times	N: normal H: HTN	Test Result		Error Rate	Times	N: normal H: HTN	Test Result		Error Rate
1	True	N	H		**2**	True	N	H		**3**	True	N	H	
	N(11)	**10**	**1**	**1/11**		N(11)	**10**	**1**	**1/11**		N(11)	**10**	**1**	**1/11**
	H(12)	**1**	**11**	**1/12**		H(12)	**0**	**12**	**0**		H(12)	**1**	**11**	**1/12**
4	True	N	H		**5**	True	N	H		**6**	True	N	H	
	N(11)	**11**	**0**	**0**		N(11)	**11**	**0**	**0**		N(11)	**10**	**1**	**1/11**
	H(12)	**0**	**12**	**0**		H(12)	**0**	**12**	**0**		H(12)	**0**	**12**	**0**
7	True	N	H		**8**	True	N	H		**9**	True	N	H	
	N(11)	**11**	**0**	**0**		N(11)	**11**	**0**	**0**		N(11)	**11**	**0**	**0**
	H(12)	**0**	**12**	**0**		H(12)	**2**	**10**	**2/12**		H(12)	**0**	**12**	**0**
10	True	N	H											
	N(11)	**10**	**1**	**1/11**										
	H(12)	**1**	**11**	**1/12**										

Table 3-10 "Optimal" Training Subset Derived from Two Jackknife Error Estimations.

Normal #	No	Training *error#*		Optimal Training Data Based on combination of **A&B**
		A. Momentum	B. Without momentum	
2	1	**V**	**V**	**V**
3	2		**V**	**V**
4	3	**V**	**V**	**V**
5	4			
6	5			
7	6	**V**	**V**	**V**
8	7			
10	8			
13	9			
23	10			
24	11	**V**	**V**	**V**
HTN				
9	1	**V**	**V**	**V**
11	2			
12	3	**V**	**V**	**V**
14	4			
15	5			
16	6			
17	7			
18	8	**V**		**V**
19	9		**V**	**V**
20	10	**V**		**V**
21	11			
22	12	**V**	**V**	**V**
Total		**9**	**9**	**11**

Table 3-11 ANN Initial Weights Trained by 11 Optimal Sample.

ANN Initial Weights without Momentum Initial learning rate $\eta = 0.01$
Iw{1,1}-Weight to layer 1 from input 1
[0.48063 -0.0054258 -0.017489 -0.12276 0.24704; -0.24552 0.12954 -0.16544 0.21916 0.11931; 0.11594 0.1031 0.13123 0.65863 -0.19268]
Iw{2,1}-Weight to output layer
[-0.21634 0.99912 0.95653]
b{1}-Bias to layer 1
[-6.5624; -0.19483; -2.9812]
b{2}-Bias to layer 2
[0]

Table 3-12 ANN Final Weights Trained by 11 Optimal Sample.

ANN Final Weights without Momentum Initial learning rate η = 0.01
Iw{1,1}-Weight to layer 1 from input 1
[-0.053048 -0.21676 1.2021 -0.40867 -0.70051; 0.17839 1.001 -0.51442 -0.69621 -0.092139; -0.054465 -0.25143 0.15553 -0.72695 -0.2211]
Iw{2,1}-Weight to output layer
[1.7635 -1.3617 -1.9717]
b{1}-Bias to layer 1
[6.0173; -2.0344; 8.5413]
b{2}-Bias to layer 2
[1.38]

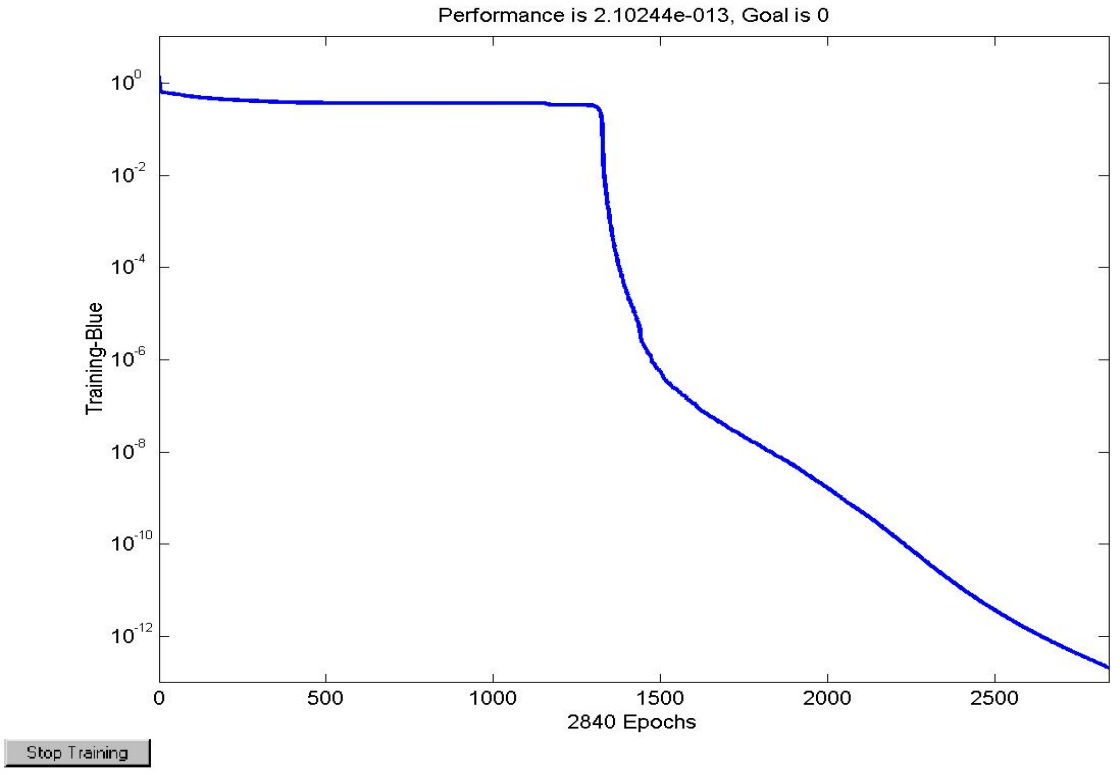

Figure 3-5 Learning Curve (with momentum) of ANN Trained by 11 Optimal Data.

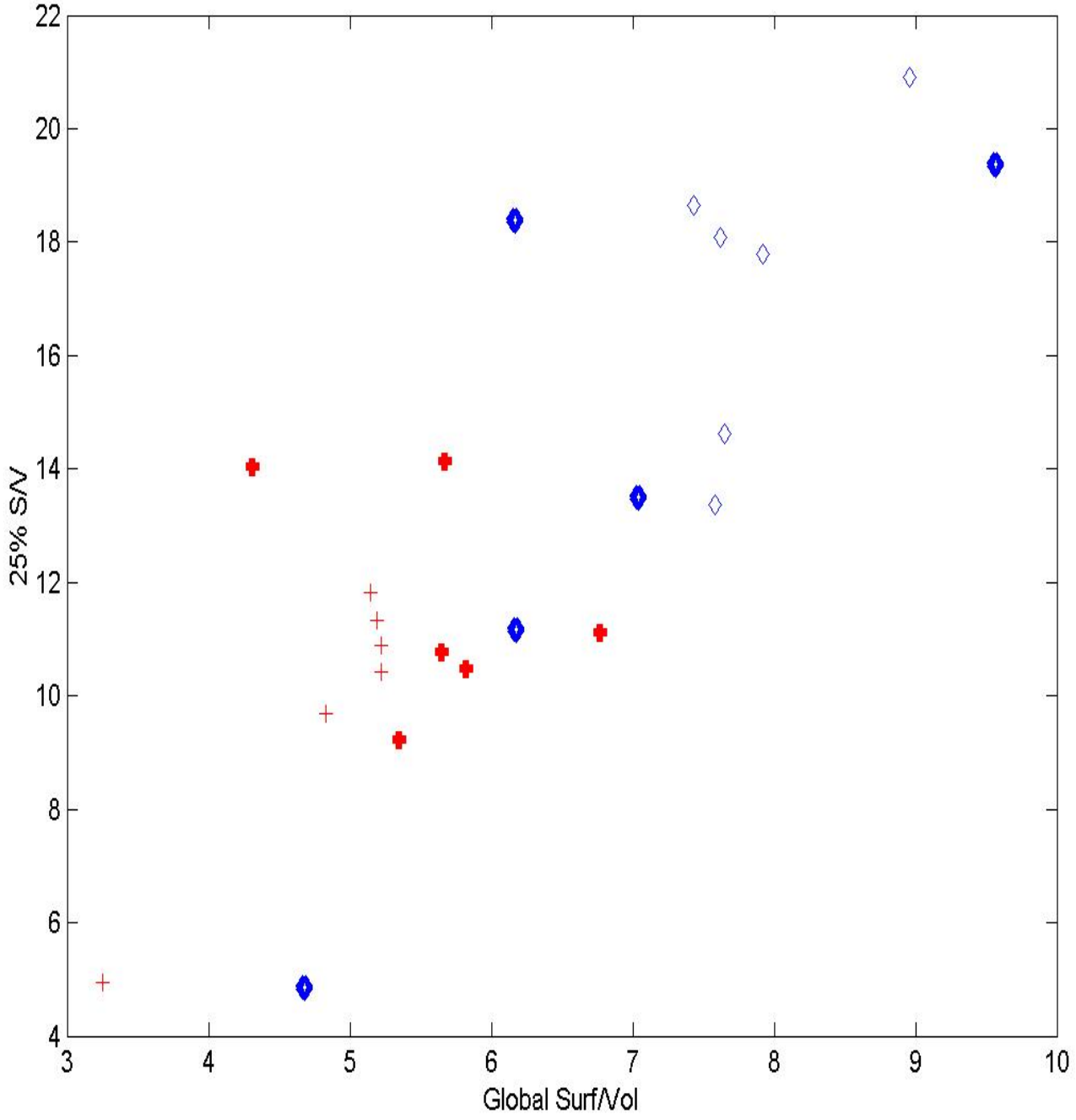

Figure 3-6 Two dimensional plot of "Optimal" Training Samples (Bold) Given in Table 3-10.

3.2 RADIAL BASIS FUNCTION NETWORKS

Radial basis function (RBF) network is one type of feedforward artificial neural network where the interpolation nonlinear activation function in each neural unit is given by a symmetric function of the form

$$f(\|x - \mathbf{c}_i\|) \qquad (3\text{-}12).$$

The argument of the function is the Euclidean distance of the input vector $\boldsymbol{x}$ from a center vector $\boldsymbol{c_i}$, which gives the name radial basis function. Two choices of the function $\boldsymbol{f}$ are

$$f(x) = e^{-\frac{\|x-\mathbf{c}_i\|^2}{2\sigma_i^2}}, \quad i = 1,\ldots, k \qquad (3\text{-}13),$$

$$f(x) = \frac{\sigma^2}{\sigma^2 + \|x - \mathbf{c}_i\|^2}, \quad i = 1,\ldots, k \qquad (3\text{-}14).$$

The Gaussian form (3-13) is more widely used. With a sufficiently large k, the decision function g($\boldsymbol{x}$) can be approximated by a linear combination of k RBFs where each is located at a different point in the space [12] [13]

$$\begin{aligned} g(x) &= \sum_{i=1}^{k} w_i e^{-\frac{(x-\mathbf{c}_i)^T(x-\mathbf{c}_i)}{2\sigma_i^2}} + b \\ &= w^T y + b \end{aligned} \qquad (3\text{-}15),$$

where y is the output vector of k RBFs. Note that g(x) is locally maximum when $\boldsymbol{x} = \boldsymbol{c_i}$. The center vector $\boldsymbol{c_i} = c_{1i}, \ldots, c_{Ni}$ of the ith hidden neuron has N components to match the input feature vector. The parameter σ_i in Equation (3-13) is used to control the spread of the radial

basis function so that its value decreases more slowly or more rapidly as x moves away from the center vector $\boldsymbol{c_i}$, that is, as $\left\|x_i - c_i\right\|$ increases.

A radial basis function network contains the following: (a) an input layer of d branching nodes, one for each feature component $\boldsymbol{x_i}$; (b) a hidden layer of M neurons where each neuron has the radial basis function $y_m = f_m(\boldsymbol{x})$ as its activation function centered at a cluster center in the feature space; and (c) an output layer of J neurons that sum up the outputs y_i from the hidden neurons, that is, each output layer neurons with output z_j uses a linear activation function

$$z_j = \sum_{m=1}^{M} w_{mj} y_m + b_j \qquad \text{(3-16).}$$

Figure 3.6 shows the block diagram of a general RBF network.

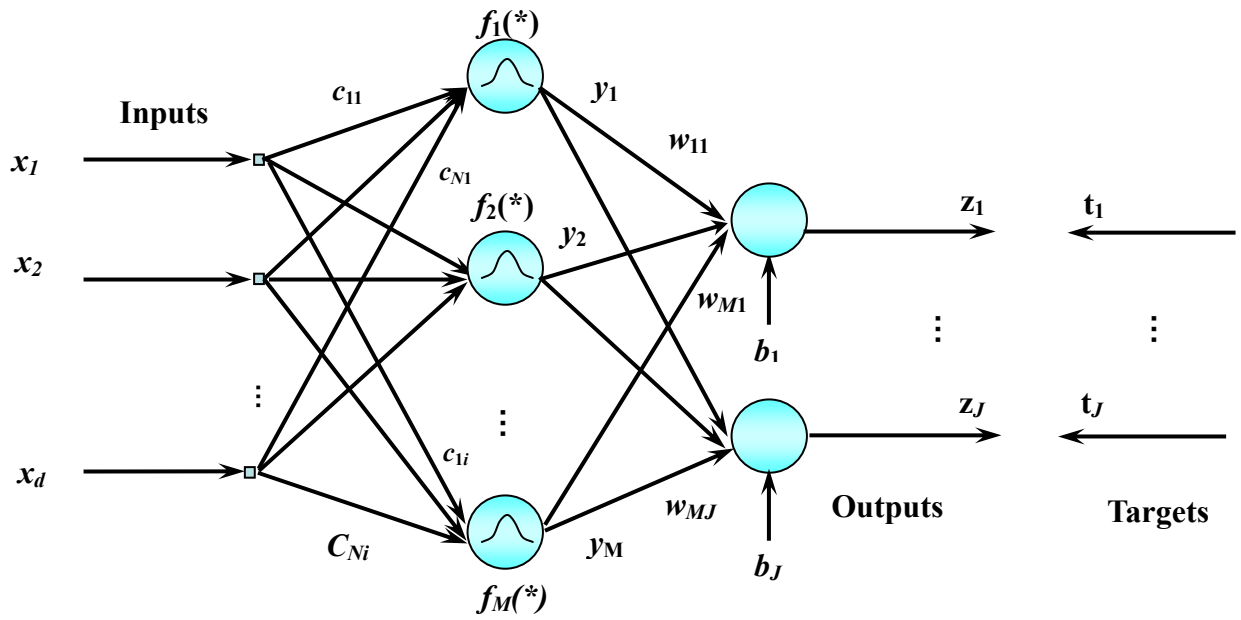

Figure 3-7 Block Diagram of a RBF Network.

In multilayer perceptrons, each hidden neuron reveals a linear combination of input features, $\sum w_i x_i$, its output will be the same for all $\boldsymbol{x}$ lying on a hyperplane $\sum w_i x_i =$ a constant. On the other hand, in the RBF networks, the output of each RBF neuron is the same for all $\boldsymbol{x}$'s that are equally distant from its center $\boldsymbol{c_i}$ and decreases exponentially (for Gaussians) with the distance. In other words, the activation responses of the neurons are of a local nature in RBF networks and of a global nature in multilayer perceptron networks. This difference makes great consequences on both the speed of convergence in training and the performance of generalization. Mainly, multilayer perceptrons learn slower than RBF networks. Simulation results have [14] shown that, in order to achieve a performance similar to that of multilayer perceptrons, an RBF network should be of much higher order. The reason is the locality of the RBF activation functions, which makes it necessary to use a large number of centers to fill in the input space in which g($\boldsymbol{x}$) is defined, and there is an exponential dependence between this number and the dimension of the input space.

The training of a RBF network involves learning these sets of parameters: $\boldsymbol{c}_m$, σ_m^2, (m = 1, 2, …, M), and connection weights $\boldsymbol{w}_{mj}$, (m = 1, 2, …, M, j = 1, 2, ,…, J), from hidden neurons to output neurons. The number of RBF to be used must be heuristically determined first. Use a set of Q training samples, $\boldsymbol{x}_q$, (q = 1, 2, …, Q), we define the total sum squared error E over all Q samples,

$$E = \sum_{q=1}^{Q} \sum_{j=1}^{J} (t_j^q - z_j^q)^2 \qquad \text{(3-17)},$$

and use the steepest descent for iteratively adjusting those parameters [15]:

$$w_{mj}(k+1) = w_{mj}(k) - \eta_1 \frac{\partial E}{\partial w_{mj}}$$

$$c_{mi}(k+1) = c_{mi}(k) - \eta_2 \frac{\partial E}{\partial c_{mi}}, \quad (i = 1, 2, ..., \mathrm{d}) \qquad (3\text{-}18).$$

$$\sigma_m^2(k+1) = \sigma_m^2(k) - \eta_3 \frac{\partial E}{\partial \sigma_m^2}$$

3.2.1 Training

A specific choice for the initial centers was suggested [16] in some cases considering the problem nature. These centers may be selected randomly from the training set which is presumed to be distributed in a meaningful manner over the input feature space.

For the right ventricle shape classification, only one output neuron is needed for two classes (normal and HTN), furthermore, it is not necessary to have a bias b_0. For the small size of the training set that we have, choosing the initial centers randomly from the training samples often failed to succeed to give a satisfactory decision function. We performed an exhaustive experimental study on the training and finally used 11 RBFs with the same spread σ. A total of [5×11 + 11 + 1 = 67] parameters were trained. Using all 23 training samples, the successfully trained network is given by the parameters listed in Table 3-13. The training convergence was reached in 11 epochs (see Figure 3-7). The decision function is given by

$$g(x) = \sum_{i=1}^{11} w_m e^{-\frac{1}{2\sigma^2}\|x - c_i\|^2} \qquad (3\text{-}19).$$

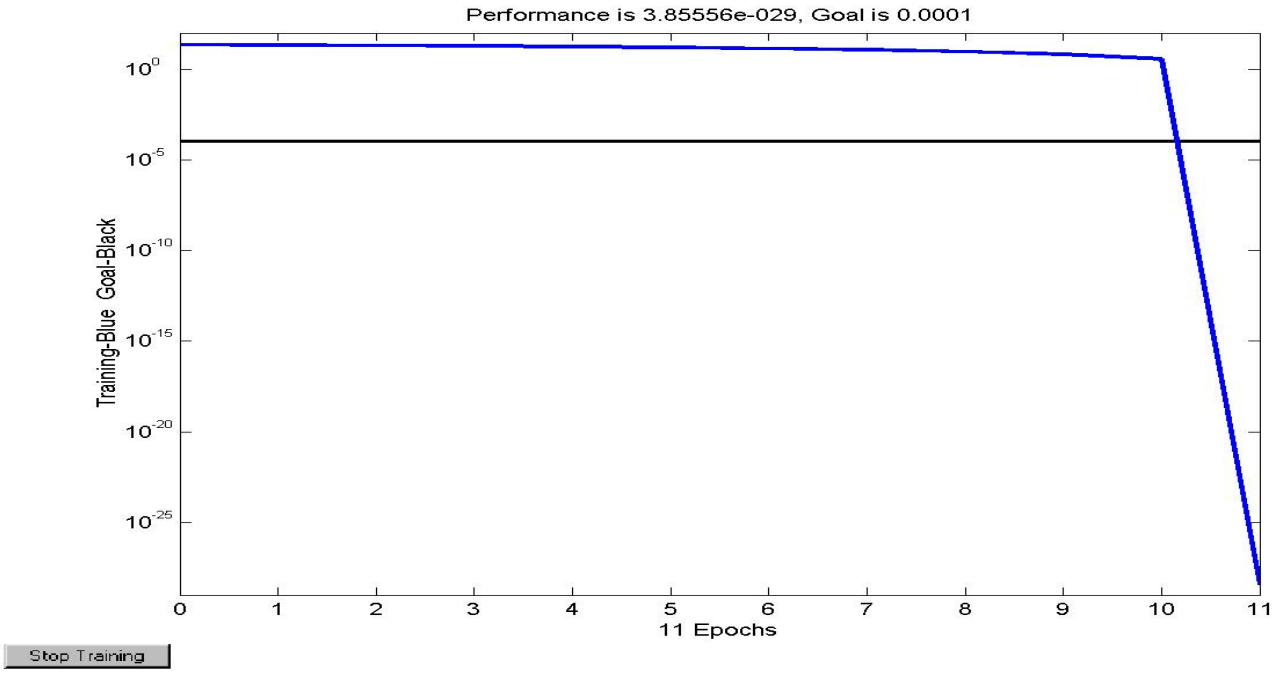

Figure 3-8 Learning Curve of the RBF Network.

Table 3-13 Final Weights of RBF Network.

Final Weights of RBF network $\sigma = 0.1, \eta_1 = 1.6, \eta_2 = 1, \quad \eta_3 = 1,$
Iw{1,1}-Weight to layer 1 from input 1
[4.68 4.85 3.87 3.7 10.26;
6.18 11.17 4.92 5.81 8;
9.57 19.36 17.85 5.66 7.84;
7.62 18.08 9.73 5.83 6.02;
7.65 14.61 7.87 6.24 6.48;
7.04 13.49 6.88 5 12.19;
7.92 17.79 11.37 5.69 8.59;
7.58 13.38 6.08 6.86 8.95;
7.43 18.66 10.16 5.33 9.37;
8.96 20.9 12.85 5.65 10.42;
6.17 18.39 8.95 5.18 4.6]
Iw{2,1}-Weight to layer
[1 1 1 1 1 1 1 1 1 1 1]

3.2.2 RBF Jackknife Error Estimation

Table 3-14 shows the Jackknife error analysis result of our RBF network. The False Positive and False Negative are

$$\text{False Positive:} \quad \frac{1}{10} \times \frac{5}{11} = \frac{5}{110} = 0.0454$$

$$\text{False Negative:} \quad \frac{1}{10} \times \frac{5}{12} = \frac{5}{120} = 0.0417$$

These two values are about the same as that obtained from the ANN trained without momentum except here the speed of convergence is much faster.

Table 3-14 False Positive and Negative Rates of RBF Jackknife Error Estimates.

Times	N: normal H: HTN	Test Result		Error Rate	Times	N: normal H: HTN	Test Result		Error Rate	Times	N: normal H: HTN	Test Result		Error Rate
1	True	N	H		2	True	N	H		3	True	N	H	
	N(11)	10	1	1/11		N(11)	11	0	0		N(11)	11	0	0
	H(12)	0	12	0		H(12)	1	12	1/12		H(12)	1	11	1/12
4	True	N	H		5	True	N	H		6	True	N	H	
	N(11)	10	1	1/11		N(11)	10	1	1/11		N(11)	11	0	0
	H(12)	0	12	0		H(12)	0	12	0		H(12)	1	11	1/12
7	True	N	H		8	True	N	H		9	True	N	H	
	N(11)	11	0	0		N(11)	10	1	1/11		N(11)	10	1	1/11
	H(12)	1	11	1/12		H(12)	0	11	0		H(12)	0	12	0
10	True	N	H											
	N(11)	11	0	0										
	H(12)	1	11	1/12										

3.3 SUMMARY OF RESULTS

Our experimental results show that the speed of convergence of the ANN (with sigmoidal functions) is much slower than the RBF network. However, in our ANN, only 3 hidden neurons are used versus 11 hidden neurons required in our RBF network for correct classification of all the training samples. With the small size of our training set, data distribution is unclear, so the RBF network needs more than triple hidden neurons. The number of parameters to be trained is many more, hence the trained result would be less certain.

A sigmoidal neuron can respond over a large region in the input space, while a radial basis neuron only responds to a relatively small region in the input space. Hence the larger is the input space (in terms of the number of inputs and the range in which those inputs may vary), more radial basis neurons are required. In the next chapter, we will discuss our study on training support vector machines employing RBF neurons and sigmoidal neurons.

4.0 SUPPORT VECTOR MACHINES

The idea behind the support vector machines is to look at the RBF network as a mapping machine, through the kernels, into a high dimensional feature space. Then a hyperplane linear classifier is applied in this transformed space utilizing those patterns vectors that are closest to the decision boundary. These are called support vectors corresponding to a set of data centers in the input space. The hyperplane in this feature space (or the nonlinear decision surface in the original space) will be optimized in giving the largest tolerance margin. The algorithm computes all the unknown parameters automatically including the number of these centers. In the last decade, significant advances have been made in support vector machine (SVM) research [17], both theoretically using statistical learning theories [18], [19], and algorithmically based on optimization techniques [20]. Since this is a relatively new design methodology for pattern classification, we give a substantially detailed review in this section, and then present a case study on right ventricle shape data.

4.1 LINEAR SUPPORT VECTOR MACHINES

Consider the 2-class problem and suppose that N training samples $\{x_i\}$ are given which are linearly separable in the feature space. Let the class index be denoted by t_i (i = 1, 2), where t_i =1 for patterns of class 1 and t_i =2 for patterns of class 2. t_i also represents the desired target output, then, we denote the training samples by $\{(x_i, t_i)\}_{i=1}^{N}$.

A linear separating plane is given by

$$g(\boldsymbol{x}) = \boldsymbol{w}^{\boldsymbol{T}}\boldsymbol{x} + b = 0 \qquad (4\text{-}1),$$

where $\boldsymbol{w}$ is a weight vector and b is a bias which determines its location related to the origin of the input space. For a given w and b, the *margin of separation* denoted by r is defined as the separation between the hyperplane in Eq. (4-1) and the closest data point as shown in Fig. 4-1, To find the optimal separating hyperplane with the largest margin is the goal of training a support vector machine. We expect that the larger the margin is, the better the classifier will be. Let $\boldsymbol{w_o}$ and b_o denote the optimal values of the weight vector and bias, respectively, the optimal hyperplane is then given by

$$g(\boldsymbol{x}) = \boldsymbol{w_o}^{\boldsymbol{T}}\boldsymbol{x} + b_o = 0 \qquad (4\text{-}2).$$

The distance from a hyperplane to a pattern $\boldsymbol{x}$ is given by

$$r = \frac{|g(x)|}{\|w_o\|} \qquad (4\text{-}3),$$

then, for all training patterns $\boldsymbol{x}$,

$$|g(x)| = |w_o^T x + b_o| = r\|w_o\| > 0 \qquad (4\text{-}4),$$

we want to find the weight vector $\boldsymbol{w_o}$ and b_o that maximizes r. The solution can be arbitrarily scaled, so we may put the constraint after an appropriate scaling as

$$\begin{aligned} w_o^T x_i + b_o &\geqslant 1 \quad \text{for } t_i = +1 \\ w_o^T x_i + b_o &\leqslant -1 \quad \text{for } t_i = -1 \end{aligned} \qquad (4\text{-}5),$$

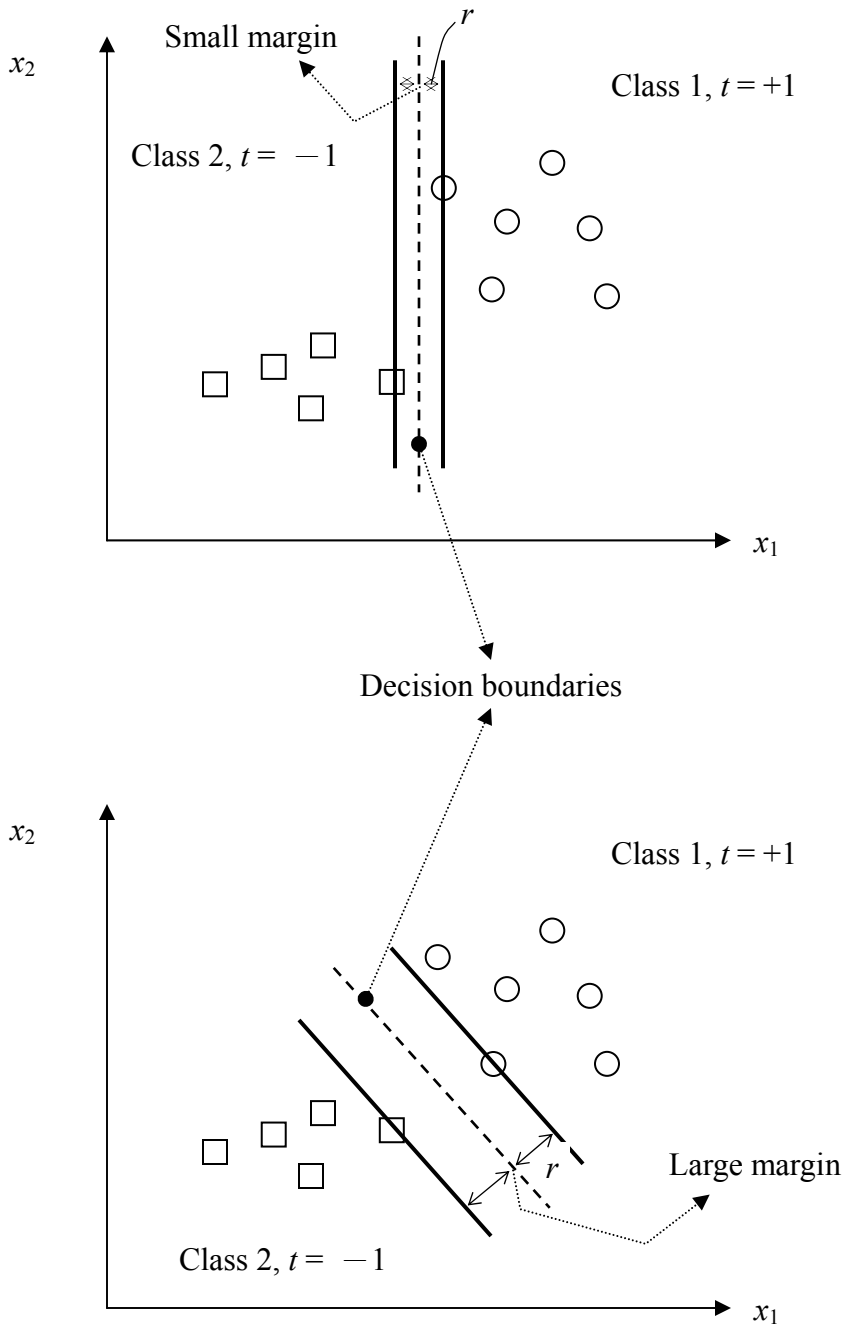

Figure 4-1 Two out of Many Separating Lines: Upper, a Less Acceptable One with a Small Margin, And Below, a Good One with a Large Margin.

From Eq. (4-4), maximizing r means minimizing $\|w_o\|^2$ under the constraints given by Eq. (4-5).

The particular points ($\boldsymbol{x_i}$, t_i) for which Eq. (4-5) is satisfied with the equality sign are called *support vectors*; they are the most difficult patterns to classify and are the training samples that will define the optimal separating hyperplane. Generally speaking, they are the most informative patterns for the classifier that we would like to design.

4.1.1 Leave-One-Out Bound

A support vector machine can be trained by choosing the current worst-classified patterns which are often the ones on the wrong side of the current decision boundary and farthest from the boundary. However, finding the worst-case patterns is computationally expensive. Before we discuss the training of a SVM, let us consider the error of such a classifier. Let N_s denote the total number of support vectors. Then for N training patterns the expected value of the generalization error rate is bounded according to [18]

$$\mathbf{E_n}\{\varepsilon\} \leq \frac{\mathbf{E}_n(N_s)}{N} \qquad (4\text{-}6),$$

where the expectation is taken over all the training set of size N drawn from the distributions which describe the categories. Leave-one-out method is usually used for evaluating the probability of testing error obtained by the empirical risk. Let us train an SVM on N-1 of the available samples, and test it on the single remaining sample. If the remaining sample happens to be a support vector for the full N sample case, there may be an error. Otherwise, there will not be.

If there exists a SVM that that will separates all the samples successfully, and the number of support vectors is small, then the expected error rate given in Eq. (4-6) will be low.

Figure 4-1 compares the idea that a classifier with a smaller margin will have a higher expected risk. The dashed separation line shown in the lower graph will promise a better performance in generalization than the dashed decision surface having a smaller margin shown in the upper graph.

4.1.2 Training a SVM

Return to the margin maximization (or $\|w_o\|^2$ minimization) problem discussed earlier, we consider the cost function to be minimized:

$$\Psi(w) = \frac{1}{2} w^T w$$

We want to find an optimal hyperplane specified by ($\boldsymbol{w}_o$, b_o) using the training sample set $\{(x_i, t_i)\}_{i=1}^{N}$.

Under the constraints in Eq. (4-5) which is equivalent to

$$t_i(w^T x_i + b) \geq 1 \qquad \text{for } i = 1,2, \ldots, N \qquad (4\text{-}7),$$

using Lagrange multipliers [21] we convert the constrained optimization problem into an unconstrained minimization problem by constructing the cost function

$$J(w,b,\alpha) = \frac{1}{2} w^T w - \sum_{i=1}^{N} \alpha_i [t_i(w^T x_i + b) - 1] \qquad (4\text{-}8),$$

where auxiliary nonnegative variables $\alpha_i \geq 0$ are called Lagrange multipliers. We seek to minimize $\boldsymbol{J}(.)$ with respect to the weight vector $\boldsymbol{w}$ and b, and maximize it with respect to $\alpha_i \geq 0$. The last term in Eq. (4-8) expresses the goal of classifying the training sample correctly. It can be shown that using the Kuhn-Tucker construction that this optimization can be reformulated as maximizing a dual form

$$Q(\alpha) = \sum_{i=1}^{N} \alpha_i - \frac{1}{2} \sum_{i=1}^{N} \sum_{j=1}^{N} \alpha_i \alpha_j t_i t_j x_i^T x_j \qquad (4\text{-}9),$$

subject to the constraints

(1) $\sum_{i=1}^{N} \alpha_i t_i = 0$

(2) $\alpha_i \geq 0 \qquad$ for $i = 1, 2, \ldots, N$

4.2 LINEAR SOFT MARGIN CLASSIFIER FOR OVERLAPPING PATTERNS

Now let us consider the case of sample patterns that not linearly separable. To find a hyperplane with a maximal margin, we must allow some sample (or samples) to be unclassified, i.e., on the wrong side of a decision boundary. In this case, we would like to find an optimal hyperplane that minimizes the probability of classification error, averaged over the training set. Thus, we will allow a *soft margin*, and those samples inside this margin are ignored. The width of a soft margin will be controlled by a regularization or corresponding penalty parameter C that determines the trade-off between the training error and the so called VC dimension of the model.

The optimal margin problem is reformulated by the introduction of non-negative slack variables ξ_i such that, instead of fulfilling Eq. (4-7), the separating hyperplane must satisfy

$$t_i(w^T x_i + b) \geq 1 - \xi_i, \quad \xi_i \geq 0 \qquad \text{for } i = 1, 2, \ldots, N, \quad . \qquad (4\text{-}10).$$

where for a sample pattern x_i, misclassified by the hyperplane, ξ_i must be greater than 1 ($\xi_i > 1$). The objective function is changed to

$$\Phi(w, \xi) = \frac{1}{2} w^T w + C \sum_{i=1}^{N} \xi_i \qquad (4\text{-}11).$$

with a regulation parameter C > 0. The inequality constrains is given by Eq. (4-10). Using Lagrange multiplier $\alpha_i \geq 0$ and $\gamma_i \geq 0$, the corresponding cost function becomes

$$J(w, b, \alpha, \gamma) = \frac{1}{2} \mathrm{w}^T \mathrm{w} + \mathrm{C} \sum_{i=1}^{N} \xi_i - \sum_{i=1}^{N} \alpha_i [t_i (\mathrm{w}^T x_i + b) - 1 + \xi_i] - \sum_{i=1}^{N} \gamma_i \xi_i \qquad (4\text{-}12).$$

Its dual form $Q(\alpha)$ for minimization is practically the same as Eq. (4-9) except for the modified bound of Lagrange multipliers α_i (constraints: $\sum_{i=1}^{N} \alpha_i t_i = 0$ and $\mathrm{C} \geq \alpha_i \geq 0$). The parameter C is the upper bound on α_i determined by the user.

4.3 NONLINEAR SUPPORT VECTOR MACHINES

The above discussion can be extended to nonlinear decision hyper surfaces for classification of nonlinearly separable data. Consider an appropriate nonlinear mapping of input

vectors into a high-dimensional feature space illustrated in Fig. 4-2 such that an optimal hyperplane can be constructed in this space. This will lead to a nonlinear support vector machine giving optimal nonlinear hypersurface in the input space.

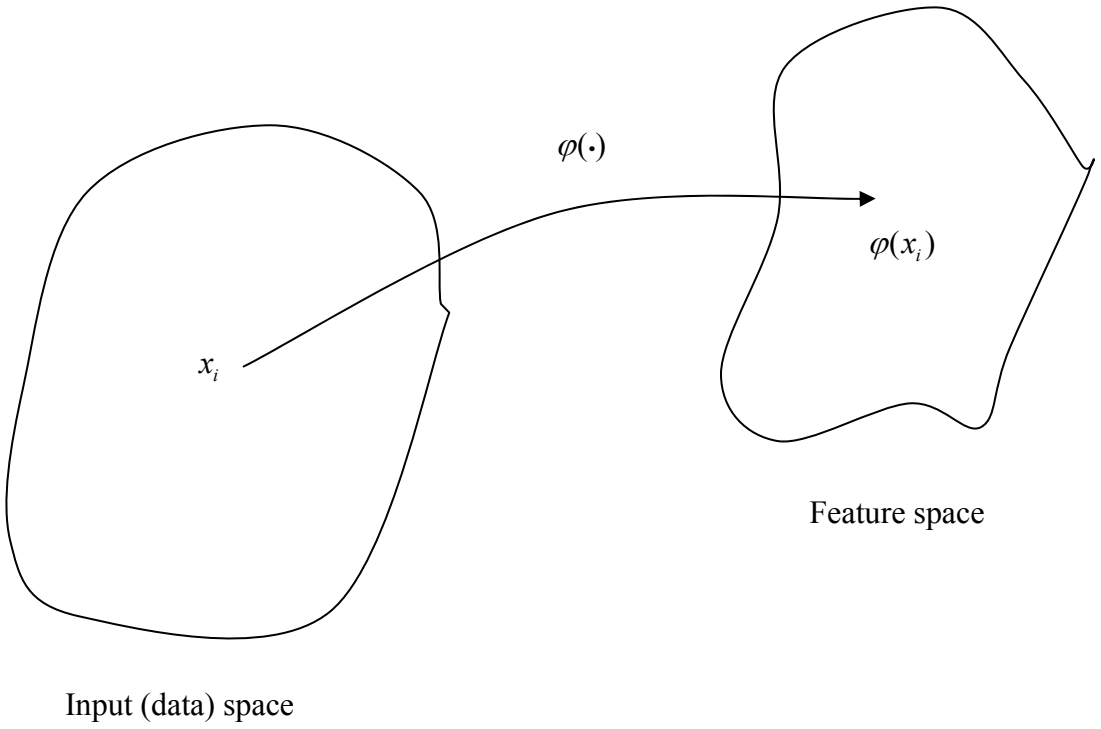

Figure 4-2 Nonlinear Mapping $\varphi(\cdot)$ from the Input Space to a High-Dimensional Feature Space.

4.3.1 Inner-Product Kernel

Let $\{\varphi_j(\mathrm{x})_{j=1}^{M}\}$ denote a set of nonlinear transformations from the input space to the feature space: M is the dimension of the new feature space. Given such a set of nonlinear transformations, we may define a hyperplane acting as the decision surface as follows:

$$\sum_{j=1}^{M} w_j \varphi_j(\mathrm{x}) + b = 0 \qquad (4\text{-}13),$$

where $\{w_j\}_{j=1}^{M}$ denotes a set of weights connecting the new feature space to the output space, and b is the bias. Augmented by $\varphi_0(\mathbf{x}) = 1$ for all $\mathbf{x}$ and w_0 as the bias b, Eq. (4-13) becomes

$$\sum_{j=0}^{M} w_j \varphi_j(\mathrm{x}) = 0 \qquad (4\text{-}14),$$

Define the vector

$$\boldsymbol{\varphi}(\boldsymbol{x}) = [\varphi_0(\mathrm{x}), \varphi_1(\mathrm{x}), ..., \varphi_M(\mathrm{x})]^T \qquad (4\text{-}15),$$

and the augmented weight vector

$$\mathrm{w} = [w_0, w_1, ..., w_M]^T, \qquad (4\text{-}16),$$

then the decision surface is given by

$$\mathrm{w}^T \boldsymbol{\varphi}(\boldsymbol{x}) = 0 \qquad (4\text{-}17).$$

We now seek the linear separability in the feature space $\boldsymbol{\varphi}(\boldsymbol{x})$**.** Let

$$\mathrm{w} = \sum_{i=1}^{N} \alpha_i t_i \boldsymbol{\varphi}(\boldsymbol{x_i}) \quad (4\text{-}18),$$

where the feature vector $\varphi(\mathbf{x}_i)$ corresponds to the ith input sample $\mathbf{x}_i$. Substituting Eq. (4-18) into (4-17) defines a decision surface computed in the feature space as:

$$\sum_{i=1}^{N} \alpha_i t_i \boldsymbol{\varphi}^{\boldsymbol{T}}(\boldsymbol{x_i})\, \boldsymbol{\varphi}(\boldsymbol{x}) = 0 \qquad (4\text{-}19).$$

The term $\boldsymbol{\varphi}^T(\boldsymbol{x}_i)\,\boldsymbol{\varphi}(\boldsymbol{x})$ represents the inner product of two (M+1)-dimensional vectors induced in the feature space by an input vector $\mathbf{x}$ and the ith training sample $\mathbf{x}_i$. Now, let $M = N$ and the inner-product kernel $\boldsymbol{K}(\mathbf{x}, \mathbf{x}_i)$ be formed from all N training samples ($\boldsymbol{\varphi}(\boldsymbol{x})$ be a (N+1)×1 vector)

$$\boldsymbol{K}(\mathbf{x}, \mathbf{x}_i) = \boldsymbol{\varphi}^T(\boldsymbol{x})\,\boldsymbol{\varphi}(\boldsymbol{x}_i)$$

$$= \sum_{j=0}^{N} \varphi_j(\mathrm{x})\varphi_j(\mathrm{x}_i) \qquad \text{for } i = 1, 2, \ldots, N \qquad (4\text{-}20),$$

The inner-product kernel is a symmetric function of its arguments, as shown by $\boldsymbol{K}(\mathbf{x}, \mathbf{x}_i) = \boldsymbol{K}(\mathbf{x}_i, \mathbf{x})$ for all i. Now we can use the inner-product kernel $\boldsymbol{K}(\mathbf{x}, \mathbf{x}_i)$ to construct the optimal hyperplane in the new feature space without having to consider the feature space itself in explicit form. The optimal hyperplane is now given by

$$\sum_{i=1}^{N} \alpha_i t_i K(\mathbf{x}, \mathbf{x}_i) = 0 \qquad (4\text{-}21).$$

Table 4-1 Specifications of Inner-Product Kernels.

Type of support vector machine	Inner product kernel $\boldsymbol{K}(\mathbf{x}, \mathbf{x}_i)$, $i = 1,2, \ldots, N$	Note
Radial basis function network	$e^{-\frac{1}{2\sigma^2}\|\mathbf{x}-\mathbf{x}_i\|^2}$	The width σ^2, common to all the kernels, is specified by the user.
Two-layer perceptron	$\tanh(\beta_0\mathbf{x}^T\mathbf{x}_i + \beta_1)$	Mercer's theorem (see Appendix B) is satisfied only for some values of β_0 and β_1.

4.3.2 Construction of a SVM

We can use the expansion of the inner-product kernel $\boldsymbol{K}(\mathbf{x}, \mathbf{x}')$ in (4-20) to construct a decision surface that is nonlinear in the input space but linear in the new feature space. Following Eq. (4-19) and replacing the inner-product $x_i^T x_j$ by the inner-product kernel $\boldsymbol{K}(\mathbf{x_i}, \mathbf{x_j}) = \boldsymbol{\varphi}^{\boldsymbol{T}}(\boldsymbol{x_i})\ \boldsymbol{\varphi}(\boldsymbol{x_j})$. The dual form of the constrained optimization for a nonlinear support vector machine is stated as follows [22]:

Given the training sample set $\{(x_i, t_i)\}_{i=1}^N$, find the Lagrange multipliers $\{\alpha_i\}_{i=1}^N$ that maximizes the objective function

$$Q(\alpha) = \sum_{i=1}^{N} \alpha_i - \frac{1}{2} \sum_{i=1}^{N} \sum_{j=1}^{N} \alpha_i \alpha_j t_i t_j K(\mathrm{x}_i, \mathrm{x}_j) \qquad (4\text{-}22),$$

subject to the constrains:

(1) $\sum_{i=1}^{N} \alpha_i t_i = 0$

(2) $0 \leqslant \alpha_i \leqslant C$ for $i = 1, 2, \ldots, N$

where C is a user-specified positive parameter and also the upper bond of α_i, $\boldsymbol{K}(\mathbf{x}, \mathbf{x}')$ can be viewed as the *ij*-th element of a symmetric N-by-N matrix K as shown by

$$\mathbf{K} = \{\boldsymbol{K}(\boldsymbol{x_i}, \boldsymbol{x_j})\}_{(i,j)=1}^{N} \qquad (4\text{-}23).$$

Compute the optimum values of the Lagrange multipliers, α_i (i = 1, 2, …, N). The weight vector w, connecting the new feature space to the output space is computed by

$$w = \sum_{i=1}^{N} \alpha_i t_i \, \boldsymbol{\varphi}(\boldsymbol{x_i}) \quad (4\text{-}24).$$

The block diagram of a nonlinear SVM is shown in Fig. 4-3.

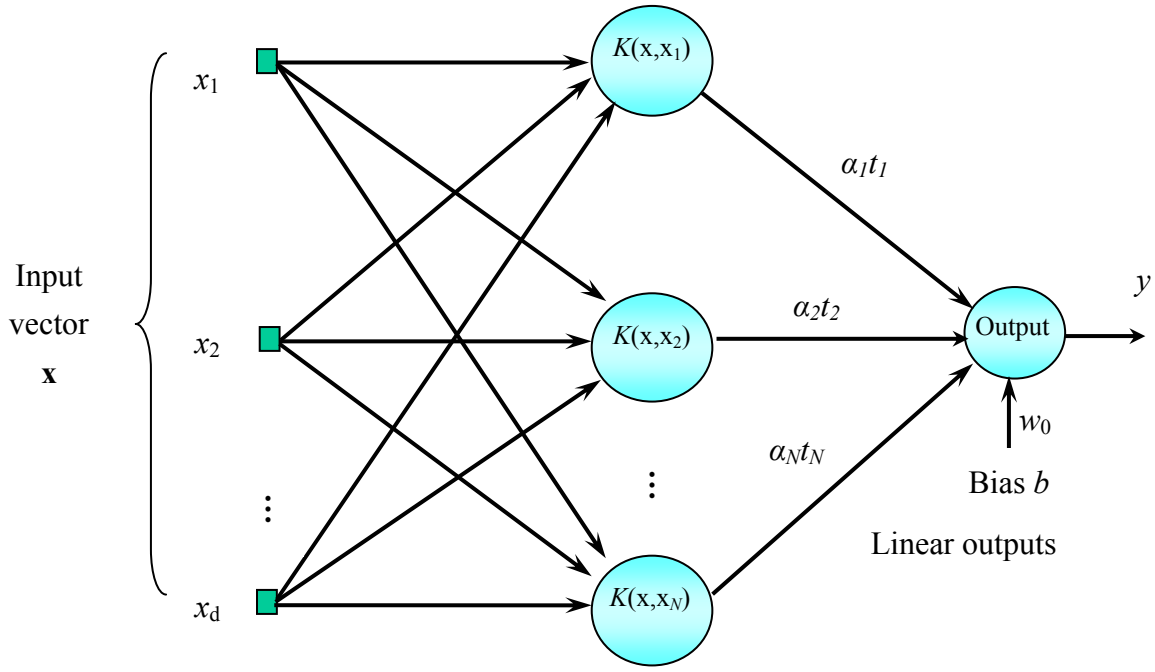

Figure 4-3 Block Diagram of a Nonlinear SVM for Training.

4.4 SUPPORT VECTOR MACHINES FOR RIGHT VENTRICLE SHAPE CLASSIFICATION

The method discussed above was applied to design SVM machines for classification of right ventricle shape measurements into normotensive or hypertensive (HTN) class [23]. We considered two kinds of kernel functions, Gaussian kernel, $\boldsymbol{K}(\mathbf{x}, \mathbf{x}_i) = e^{-\frac{1}{2\sigma^2}\|\mathbf{x}-\mathbf{x}_i\|^2}$, and sigmoidal kernels $\boldsymbol{K}(\mathbf{x}, \mathbf{x}_i) = \tanh(\beta_0 \mathbf{x}^T \mathbf{x}_i + \beta_1)$, as listed in Table 4-1. All 23 sample patterns of 5 dimensions ($\{x_i, t_i = 1 \mid i = 1, 2, \ldots, 11\}$, normal; $\{ x_i, t_i = -1 \mid i = 12, 13, \ldots, 23\}$, HTN), as given in Appendix A, were used in training, so initially there are 23 units in the hidden layer of the SVM.

For the SVM using Gaussian kernels (with $\sigma = 1$ in all units), experiments were made using different values of regularization parameter C. Note that Gaussian kernels do not necessarily require a bias term in the decision function $g(\boldsymbol{x})$, in this case, the equality constraint $\sum_{i=1}^{N} \alpha_i t_i = 0$ (which is resulted from $\frac{\partial J}{\partial b} = 0$) does not exit. The computed α_i ($i = 1, 2, \ldots, 23$) under C = 100 are shown in Table 4-2. There are 8 support vectors, those are training patterns for which $0 < \alpha_i < C$ as marked by V in the Table. All other patterns ($\alpha_i = 0$) are outside the margin strip. The set of support vectors (SV) are (x_1, x_2, x_6, x_{11}, with $t_i = 1$) and (x_{12}, x_{14}, x_{20}, x_{22}, with $t_i = -1$). The decision function is given by

$$g(\mathbf{x}) = \alpha_1 K(\mathbf{x},\mathbf{x_1}) + \alpha_2 K(\mathbf{x},\mathbf{x_2}) + \alpha_6 K(\mathbf{x},\mathbf{x_6}) + \alpha_{11} K(\mathbf{x},\mathbf{x_{11}}) - \alpha_{12} K(\mathbf{x},\mathbf{x_{12}}) - \alpha_{14} K(\mathbf{x},\mathbf{x_{14}}) - \alpha_{20} K(\mathbf{x},\mathbf{x_{20}}) - \alpha_{22} K(\mathbf{x},\mathbf{x_{22}}) \qquad (4\text{-}25),$$

Table 4-2 Results of SVM with Gaussian Kernels.

Kernel: Gaussian, σ= 1, C=100			
	No.	α_i	SVM
Normal	1	7.9237	V
	2	14.2993	V
	3	0.0000	
	4	0.0000	
	5	0.0000	
	6	10.6449	V
	7	0.0000	
	8	0.0000	
	9	0.0000	
	10	0.0000	
	11	3.1767	V
HTN	12	4.8679	V
	13	0.0000	
	14	7.9043	V
	15	0.0000	
	16	0.0000	
	17	0.0000	
	18	0.0000	
	19	0.0000	
	20	19.4704	V
	21	0.0000	
	22	1.1980	V
	23	0.0000	

where $K(\mathbf{x}, \mathbf{x}_i) = e^{-\frac{1}{2\sigma^2}(\mathrm{x}-x_i)^T(\mathrm{x}-x_i)}$

The tolerance margin is $r = \frac{1}{\|w\|}$. Since the expression of $\varphi(\mathbf{x})$ was not explicitly given, weight vector $w = \sum_{i=1}^{N} \alpha_i t_i \boldsymbol{\varphi}(\boldsymbol{x_i})$ was not computed. However, $\|w\|^2$ was computed via

$$\|\mathrm{w}\|^2 = \mathrm{w}^{\mathrm{T}}\mathrm{w} = [\sum_j \alpha_j t_j \varphi(x_j)]^T [\sum_i \alpha_i t_i \varphi(x_i)]$$

$$= \sum_{j\in SV}\sum_{i\in SV} \alpha_j t_j \alpha_i t_i \varphi^T(x_j)\varphi(x_i)] = \sum_j \sum_i \alpha_j t_j \alpha_i t_i K(x_j, x_i) \qquad (4\text{-}26).$$

Using the determined support vectors gives $\|\mathrm{w}\|^2 = 17.3712$, hence, the tolerance margin is

$$\mathrm{r} = \frac{1}{\sqrt{\|\mathrm{w}\|^2}} = 0.23993.$$

Hence, we only need 8 hidden units, instead of 23, in the trained classifier as shown in Figure 4-4. The decision boundary in x1-x2 (Global S/V, 0-25%S/V) plane with the projection of sample patterns are shown in Figure 4-5. A small margin is noticed in the graph.

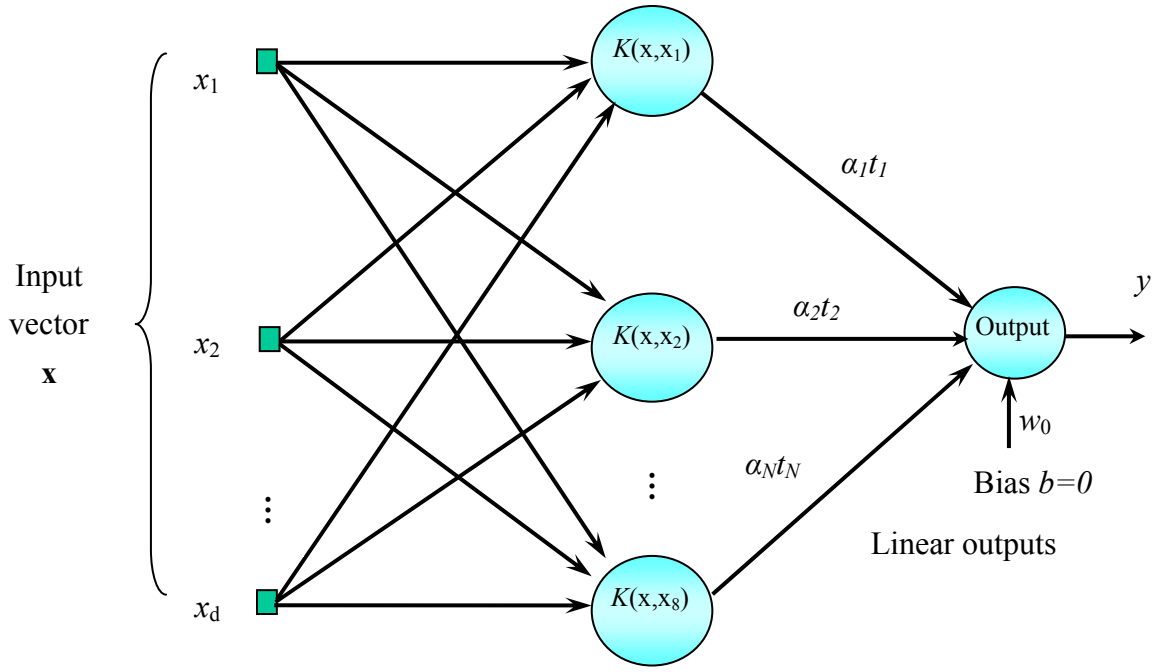

Input layer of dimension d
Use *N* testing samples

Hidden layer of 8 Inner-product kernels
$K(\mathbf{x}, \mathbf{x}_j) = \boldsymbol{\varphi}(\boldsymbol{x})\ \boldsymbol{\varphi}(\boldsymbol{x}_j)$, $j = 1, 2, \ldots, 8$

Figure 4-4 Block Diagram of the Trained SVM.

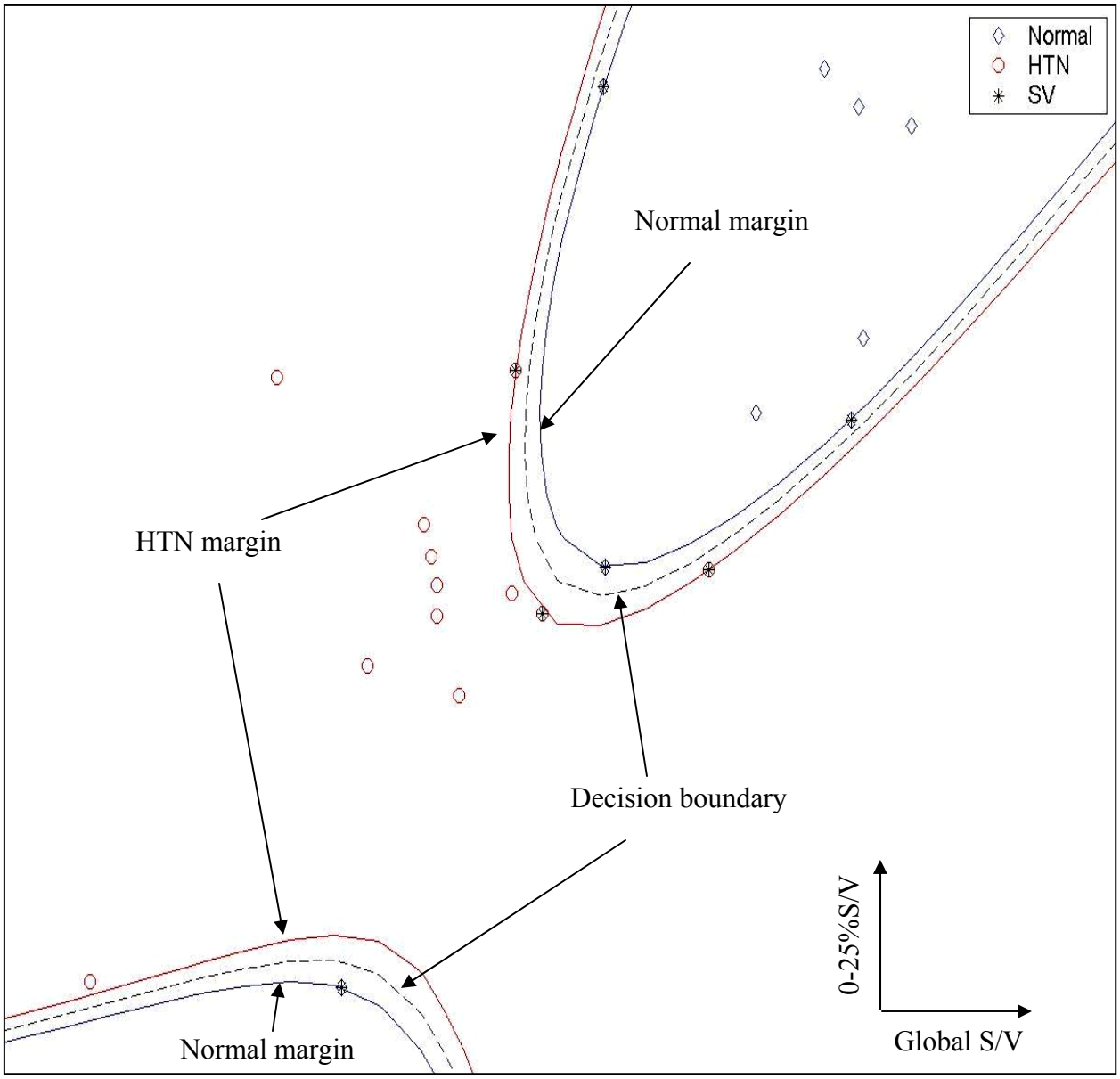

Figure 4-5 Decision Boundary in x1-x2 (Global S/V, 0-25%S/V) Plane with the Projection of Sample Patterns.

We performed the leave-one-out testing of this SVM by training on 22 samples and testing on the left-out 1 sample, rotated 23 times. The results are given in Table 4-3. The training was successful each time; there was 1 error in testing some time, whenever it was one of the support vectors obtained in the full training (training all 23 samples). The average false positive and average false negative are 0.01186 ($=\frac{1}{23}\times\frac{3}{11}$) and 0.00725 ($=\frac{1}{23}\times\frac{2}{12}$); 3 samples are classified correctly but with the margin strips.

The other SVM used sigmoidal kernel with β0 = 0.9 and β1 = 0.5, the computed α_i's under C = 100 are listed in Table 4-4. There appears to have seven support vectors ($\alpha_i > 0$), five of which computed to α_i = C = 100 (i = 1, 2, 3, 11, 12, 14, 19). Only two support vectors corresponding to $\alpha_i < C$. For those samples x_i having α_i = C = 100, the corresponding slack variables ξ_i may be greater than 0 or even 1; ξ_i can be computed from $t_i g(\boldsymbol{x_i}) = 1 - \xi_i$. For $\xi_i > 1$, the training sample must be misclassified; for $1 > \xi_i > 0$, the sample was correctly classified but close to the hyperplane with a distance less than the margin.

Compare the support vectors found in each SVM with the "optimal" training data found by the Jackknife analysis of ANN (Table 3-10), it is not surprising that all the support vectors (except pattern No. 14) of the SVM with sigmoidal kernels are members of that "optimal" training data. Similarly, the support vectors of the SVM with Gaussian kernels also coincide with that set except for pattern No. 14.

Table 4-3 Result of Leave-One-Out Testing.

Times	Leave out (testing) Pattern No.	No. of SV	Testing Pattern no. (value)		Correct value
			Error	With margin strip value	
1.	1.	6	1(-2.3185)		
2.	2.	9	2(-0.7958)		
3.	3.	8			1.1846
4.	4.	8			2.8205
5.	5.	8			3.2176
6.	6.	9	6(-1.2802)		
7.	7.	8			3.1304
8.	8.	8			3.1912
9.	9.	8			3.0087
10.	10.	8			2.4327
11.	11.	8	11	0.2091	
12.	12.	8	12	-0.0935	
13.	13.	8			-1.9708
14.	14.	8	14(1.6830)		
15.	15.	8			-2.8525
16.	16.	8			-1.7962
17.	17.	8			-2.0487
18.	18.	8			-2.8443
19.	19.	8			-2.6779
20.	20.	8	20(0.1423)		
21.	21.	8			-2.8983
22.	22.	7	22	-0.0437	
23.	23.	8			-2.0673

Table 4-4 Results of SVM with Sigmoid Kernels.

Kernel: Sigmoid, $\beta_0 = 0.9$, $\beta_1 = 0.5$, C = 100			
	No.	α_i	SVM
Normal	1	100.0000	V
	2	100.0000	V
	3	46.1821	V
	4	0.0000	
	5	0.0000	
	6	0.0000	
	7	0.0000	
	8	0.0000	
	9	0.0000	
	10	0.0000	
	11	53.8179	V
HTN	12	100.0000	V
	13	0.0000	
	14	100.0000	V
	15	0.0000	
	16	0.0000	
	17	0.0000	
	18	0.0000	
	19	100.0000	V
	20	0.0000	
	21	0.0000	
	22	0.0000	
	23	0.0000	

5.0 CONCLUSIONS AND FUTURE WORK

The case study conducted in this project is concerned with the classification of right ventricle shape measurements obtained from MRI sequences, to either normal or hypertensive classes. Pediatricians are interested in diagnosis on possible congenital heart defects, especially those associated with pressure and volume overload problems. The samples are given in 5-dimensional data, and only a small sample set are available. To develop a suitable pattern classifier, we went through first the Fisher linear discriminant and the linear classifier trained by the Ho-Kayshap algorithm. The results showed that the sample data are nonlinearly separable. We then focused on training of feedforward artificial neural networks using sigmoidal functions and radial bias functions, considering the feature dimensions, small sample size and the limit on the number of neurons to be used, we succeeded in training an ANN having only three hidden neurons (with sigmoidal nonlinearity) and one output neuron, and a RBF network with 11 Gaussian basis functions, all with 100% classification capability. Jackknife training and error estimation were performed in both cases. The issues attacked are the minimum number of units needed and the associated minimum number of parameters to be trained in comparison to an earlier study. In order to minimize the structural risk, we next considered support vector machines and trained nonlinear classifiers with minimum number of hidden neurons giving certain tolerance margins.

The artificial neural network using back-propagation training suffers from its slow convergence. They may have larger testing (statistic) errors as compared to support vector machines due to the Empirical Risk Minimization (ERM) approach employed by the former. The RBF network converges with an amazing speed. Nevertheless, with the small amount of available RV shape data for training, we were unable to reduce the number of hidden neurons used in the RBF network.

Although the SVM uses as many kernels during the training as the number of training samples when it maps nonlinearly the original data into new feature space, its support vectors were quickly found and the optimal separating surface gave the best possible tolerance margin. The resulting number of hidden neurons used is 8, more than that used in the ANN. It implies the minimization of structure risk (SRM) and minimizing the number of neural units used, through minimizing an upper bound on the generalization error as opposed to ERM which minimizes the error on the training data. Our experimental results on the case study have shown that although the ANN (sigmoidal) and SVM are comparable in performance, SVM has a greater potential to generalize in statistical learning. We would like to gather more training data to carry out further studies on the right ventricle shape classification. We also would like to investigate the automatic segmentation of right ventricles from cardiac MRI sequences to obtained real world data with the goal of developing a fully automatic pattern recognition system.

APPENDIX A

Table A-1 Sample Right Ventricle Shape Data Obtained from MRI Sequences with 11 Normal and 12 Hypertensive (HTN) Cases. Five Features Consist of Global and Four Regional Surface/Volum Ratios [2].

	Sample		Shape Features (Surface/Volum Ratio)				
	#	No.	Global S/V	25%	50%	75%	100%
Normal	2	1	4.68	4.85	3.87	3.70	10.26
	3	2	6.18	11.17	4.92	5.81	8.
	4	3	9.57	19.36	17.85	5.66	7.84
	5	4	7.62	18.08	9.73	5.83	6.02
	6	5	7.65	14.61	7.87	6.24	6.48
	7	6	7.04	13.49	6.88	5.	12.19
	8	7	7.92	17.79	11.37	5.69	8.59
	10	8	7.58	13.38	6.08	6.86	8.95
	13	9	7.43	18.66	10.16	5.33	9.37
	23	10	8.96	20.90	12.85	5.65	10.42
	24	11	6.17	18.39	8.95	5.18	4.60
HTN	9	12	5.67	14.12	7.46	4.85	4.78
	11	13	4.83	9.68	3.90	4.02	8.18
	12	14	6.77	11.12	5.58	5.89	14.13
	14	15	5.22	10.43	5.16	3.91	5.63
	15	16	5.22	10.90	4.36	3.84	9.09
	16	17	5.15	11.81	5.11	4.11	8.52
	17	18	5.19	11.33	4.86	3.87	6.31
	18	19	5.35	9.23	7.34	3.80	4.56
	19	20	5.82	10.46	4.82	4.82	9.08
	20	21	4.31	14.02	4.18	3.36	4.54
	21	22	3.25	4.94	2.90	2.79	4.18
	22	23	5.65	10.77	5.01	4.49	6.38

is the sample number assigned in Reference [2].

APPENDIX B

Mercer's Theorem

The expansion of Eq. (4-20) for the inner-product kernel $\boldsymbol{K}(\mathbf{x}, \mathbf{x}_i)$ is an important special case of Mercer's theorem that arises in functional analysis [19]. Let $\boldsymbol{K}(\mathbf{x}, \mathbf{x}')$ be a continuous symmetric kernel that is defined in the closed interval $\mathbf{a} \leq \mathbf{x} \leq \mathbf{b}$ and likewise for $\mathbf{x}'$. The kernel $\boldsymbol{K}(\mathbf{x}, \mathbf{x}')$ can be expanded in the series form

$$\boldsymbol{K}(\mathbf{x}, \mathbf{x}') = \sum_{i=1}^{\infty} \lambda_i \varphi_i(\mathrm{x}) \varphi_i(\mathrm{x}') \qquad (4\text{-}22),$$

with positive coefficients $\lambda_i > 0$ for all i. For this expansion to be valid and for it to converge absolutely and uniformly, it is necessary and sufficient that the following condition

$$\int_{\mathbf{b}}^{\mathbf{a}} \int_{\mathbf{b}}^{\mathbf{a}} K(\mathbf{x}, \mathbf{x}') \psi(\mathbf{x}) \psi(\mathbf{x}') d\mathbf{x} d\mathbf{x}' \geqslant 0$$

holds true for all $\psi(\cdot)$ for which

$$\int_{\mathbf{b}}^{\mathbf{a}} \psi^2(\mathbf{x}) d\mathbf{x} < \infty$$

The functions $\varphi_i(\mathbf{x})$ are called eigenfunctions of the expansion and the numbers λ_i are eigenvalues. The fact that all of the eigenvalues are postitive means that the kernel $\boldsymbol{K}(\mathbf{x}, \mathbf{x}')$ is positive definite. From the defining equation (4-13), we see that the support vector machine includes a form of regularization in an implicit sense. In particular, the use of a kernel $\boldsymbol{K}(\mathbf{x}, \mathbf{x}')$ defined in accordance with Mercer's theorem corresponds to the regularization with an operator D such that the kernel $\boldsymbol{K}(\mathbf{x}, \mathbf{x}')$ is the Green's function of $\widetilde{\mathbf{D}}\mathbf{D}$ where $\widetilde{\mathbf{D}}$ is the adjoint of $\mathbf{D}$ [24].

BIBLIOGRAPHY

[1] N. Cristianini and J. Shawe-Taylor. "An Introduction to Support Vector Machines", Cambridge University Press, Cambridge, 2000.

[2] M. Kaygusuz, R. Munoz, P. M. Pattany and J. Fishman, "Artificial Neural Networks: Comparing Hypertensive And Normotensive Three-Dimensional Right Ventricular Shapes Using MRI", Preprint, 2003.

[3] R. A. Fisher. "The use of multiple measurements in taxonomic problem", Annals of Eugenics, 7:179–188, 1936.

[4] Y-C. Ho, and R. L. Kashyap, An Algorithm for Linear Inequalities and its Applications, IEEE Trans, On Neural Networks, 3, pp. 51-61, 1965.

[5] K. Hornik, M. Stinchcombe, and H. White, "Multilayer feedforward networks are universal approximators", Neural Networks, 2, 359–366, 1989.

[6] B. D. Ripley, "Pattern Recognition and Neural Networks", New York, Cambridge University Press, 1996.

[7] G. Wahba, "Generalization and regularization in nonlinear learning systems", In M. A. Arbib, editor, The Handbook of Brain Theory and Neural Networks, pp. 426–430, Cambridge, MIT Press, 1995.

[8] S. E. Fahlman and C. Lebiere, "The cascade-correlation learning architecture", In D. S. Touretsky, editor, Advances in Neural Information Processing Systems, pp. 524–532, San Mateo, CA, Morgan Kaufmann, 1990.

[9] R. S. Shadafan and M. Niranjan, "A dynamic neural network architecture by sequential partitioning of the input space", Neural Computation, 6:1202–1222, 1994.

[10] Richard O. Duda, Peter E. Hart and David G. Stork , "Pattern Classification", John Wiley & Sons, Inc, pp. 117-121, 2001.

[11] MATLAB, User's Guide, The MathWorks, Inc., Natick, MA 01760, 1994-2002, http://www.mathworks.com.

[12] Broomhead D. S., Lowe D, "Multivariable functional interpolation and adaptive networks", Complex Systems, Vol. 2, pp. 321-355, 1988.

[13] J. Moody, C. J. Darken "Fast learning in networks of locally tuned processing units", Neural Computation, Vol. 6(4), pp. 281-294, 1989.

[14] E. J. Hartman, J.D. Keeler, Kowalski J. M. "Layered neural networks with Gaussian hidden units as universal approximations", Neural Computations, Vol. 2(2), pp. 210-215, 1990.

[15] S. Theodoridis, C.F.N. Cowan, C. Callender, C.M.S. Lee, “Schemes for equalization in communication channels with nonlinear impairments”, IEEE Proceedings on Communications, Vol. 61(3), pp. 268-278, 1995.

[16] Carl G. Looney, “Pattern Recognition Using Neural Networks: Theory and Algorithms for Engineers and Scientists”, Oxford University Press, NY, 1997.

[17] C. J. C. Burges. “A tutorial on support vector machines for pattern recognition”, Data Mining and Knowledge Discovery, 2(2):121–167, 1998.

[18] V. N. Vapnik, “Statistical Learning Theory”, John Wiley & Sons Inc., New York, 1998.

[19] T. Evgeniou, M. Pontil, and T. Poggio, “Regularization networks and support vector machines, Advances in Large Margin Classifiers”, pp. 171–203, Cambridge, MA, MIT Press, 2000.

[20] J. Nocedal and S. J. Wright, “Numerical Optimization”, Springer-Verlag, New York, 1999.

[21] D. P. Bertsekas, “Nonlinear Programming”, Belmont, MA: Athena Scientific, 1995.

[22] S. S. Haykin, “Neural Networks: A Comprehensive Foundation”, 2nd ed. Upper Saddle River, NJ: Prentice Hall, 1999.

[23] S. R. Gunn, “Support Vector Machines for Classification and Regression”, Technical Report, Image Speech and Intelligent Systems Research Group, University of Southampton, 1997.

[24] Smola, A. and B. Scholkopf, “A tutorial on support vector regression”, NeuroCOLT2 Technical Report NC2-TR-1998-030, 1998. http://www.neurocolt.com.